WORKSHOP ON THE POLAR REGIONS OF MARS: GEOLOGY, GLACIOLOGY, AND CLIMATE HISTORY

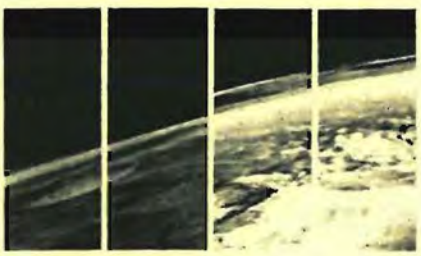

MSATT

Mars Surface and Atmosphere Through Time

LPI Technical Report Number 92-08, Part 1

LUNAR AND PLANETARY INSTITUTE 3600 BAY AREA BOULEVARD HOUSTON TX 77058-1113

LPI/TR--92-08, Part 1

WORKSHOP ON

THE POLAR REGIONS OF MARS: GEOLOGY, GLACIOLOGY, AND CLIMATE HISTORY

Edited by

S. M. Clifford, A. D. Howard, and W. S. B. Paterson

Held at
Houston, Texas

November 13–15, 1992

Sponsored by
Lunar and Planetary Institute
The MSATT Study Group

Lunar and Planetary Institute 3600 Bay Area Boulevard Houston TX 77058-1113

LPI Technical Report Number 92-08, Part 1
LPI/TR--92-08, Part 1

Compiled in 1992 by
LUNAR AND PLANETARY INSTITUTE

The Institute is operated by Universities Space Research Association under Contract NASW-4574 with the National Aeronautics and Space Administration.

This report may be cited as
Clifford S. M., Howard A. D., and Paterson W. S. B., eds. (1992) *Workshop on the Polar Regions of Mars: Geology, Glaciology, and Climate History.* LPI Tech. Rpt. 92-08, Part 1, Lunar and Planetary Institute, Houston. 30 pp.

This report is distributed by

ORDER DEPARTMENT
Lunar and Planetary Institute
3600 Bay Area Boulevard
Houston TX 77058-1113

Mail order requestors will be invoiced for the cost of shipping and handling.

PREFACE

This volume contains papers that have been accepted for the Workshop on the Polar Regions of Mars: Geology, Glaciology, and Climate History, November 13–15, 1992, in Houston, Texas. The Program Committee consisted of Steve Clifford (Lunar and Planetary Institute, Houston), Alan Howard (University of Virginia, Charlottesville), and Stan Paterson (Paterson Geophysics, Heriot Bay).

Logistics and administrative support were provided by the Program Services Department staff at the Lunar and Planetary Institute. This volume was prepared by the Publications Services Department staff at the Lunar and Planetary Institute.

CONTENTS

GLACIATION IN ELYSIUM. Duwayne M. Anderson, Texas A&M University, College Station TX 77843-3115, USA.

Results of a study of high-resolution Viking Orbiter images of the northwestern slopes of Elysium Mons, utilizing a variety of image analysis techniques, provide striking evidence of an extended period of glaciation that involved a large ice sheet of greater than 1.2 km thickness and subice fluvial activity that contributed to the formation of the channels of Hrad Valles and Granicus Valles. These two unusual channel systems begin on the lower slopes of Elysium Mons and extend into Utopia Planitia in the region lying between 215° and 230°W and between 25° and 45°N. Key indicators are the presence of serrated volcanic constructs whose dimensions and morphology indicate an origin involving successive, localized, subice fissure eruptions. The channels visible in Hrad Valles bear a striking resemblance to subice fluvial features found in the dry valleys of Antarctica at the periphery of this massive continental ice sheet. Crater size distributions and crater morphologies are quite consistent with this interpretation, as are certain other topographic features suggesting the presence in the past of ice-rich permafrost that, while having undergone significant degradation, still remains.

ORBITAL, ROTATIONAL, AND CLIMATIC INTERACTIONS: LESSONS FROM EARTH AND MARS. Bruce G. Bills, Geodynamics Branch, NASA Goddard Space Flight Center, Greenbelt MD 20771, USA.

Introduction: Though variations in orbital and rotational parameters of the Earth and Mars are widely recognized as plausible sources of significant climatic variation on 10^3–10^8-yr timescales, many aspects of the connection between orbital, rotational, and climatic variations remain poorly understood. In general, the orbital histories are very well known, the rotational histories are less well known, and the climatic histories (especially for Mars) are very poorly known. A brief review will be given of recent progress in computing orbital and rotational secular variations, and in connecting them to climatic change. The emphasis will be on highlighting those areas that limit our present understanding.

It is obvious that mass redistributions associated with climatic change (glaciations) are an important source of crustal deformation and geodynamic change on the Earth, and may have played a similar role on Mars in the distant past. It is much less widely appreciated, however, that rates, phases, and amplitudes of deformation of the deep interior of the planet can influence climate. The mantle and core, if completely decoupled, would precess at quite different rates, and even with plausible coupling strengths, some degree of differential precession is possible. Mass flow associated with glaciations can influence the precessional dynamics of the Earth or Mars, and changes in orbital and rotational parameters influence the latitudinal and seasonal pattern of insolation. Previous attempts to account for astronomically forced climatic change have usually only considered extremely simplisitic models for the response of the solid planet to external torques and surface loads.

The Traditional Perspective: The latitudinal and seasonal pattern of incident solar radiation depends on the eccentricity of the planetary orbit and the orientation of the spin axis relative to both the orbit normal and the aspidal line. Unit vectors $\mathbf{s}$ and $\mathbf{n}$ characterize the directions of the spin axis and orbit normal respectively. Two angles completely characterize the relative orientation of the spin axis. The obliquity ε is simply the angle between the orbit normal and the spin axis

$$\varepsilon = \cos^{-1}(\mathbf{n}\cdot\mathbf{s}) \tag{1}$$

The ascending node of the orbit plane on the instantaneous equator plane has an orientation given by $(\mathbf{s}\times\mathbf{n})$, and the longitude of perihelion ϖ is just the angle in the orbit plane from that node to perihelion. It is widely appreciated that secular variations in these three parameters (e,ε,ϖ) produce major climatic change [1,2]. In fact, spectral analyses of long, high-resolution marine sediment isotopic records show significant variance at periods near 100 kyr, 41 kyr, and 19–23 kyr, which are generally attributed to spectral lines in the radiative forcing fluctuations associated with e, ε, and $e\sin(\varpi)$ respectively.

The causes and effects of the orbital changes are quite well understood. Gravitational interactions with the other planets cause the shape and orientation of the orbit to change on timescales of 10^4–10^6 yr. The inclination I and nodal longitude Ω determine the orientation of the orbit plane. The eccentricity e and perihelic longitude ω determine the shape of the orbit and its orientation within the plane. Note that ω is measured from an inertially fixed direction, rather than the moving node as is the case for ϖ. The secular evolution of the orbital element pairs (I,Ω) and (e,ω) can be conveniently represented in terms of Poisson series

$$\begin{aligned} p &= \sin(I)\sin(\Omega) = \Sigma N_j \sin(s_j t + g_j) \\ q &= \sin(I)\cos(\Omega) = \Sigma N_j \cos(s_j t + g_j) \end{aligned} \tag{2}$$

$$\begin{aligned} h &= e\sin(\omega) = \Sigma M_j \sin(r_j t + f_j) \\ k &= e\cos(\omega) = \Sigma M_j \cos(r_j t + f_j) \end{aligned} \tag{3}$$

In the lowest-order solution, there are as many frequencies r_j and s_j as there are planets. However, the frequencies r_j and s_j are characteristic modal frequencies (eigenvalues) of the coupled system of oscillators and are not each uniquely asso-

ciated with a particular planet [3]. The frequencies r_j are all positive, indicating that the perihelia advance. In the lowest-order solution, the apsidal rates are all in the interval ($0.667 < r_j < 28.221$ arcsec/yr). The corresponding periods are 45.92 kyr to 1.943 m.y. One of the frequencies, s_j, is zero, and all the others are negative, indicating that the nodes regress. In the lowest-order solution, the nonzero nodal rates are all in the interval ($0.692 < s_j < 26.330$ arcsec/yr). The corresponding periods are 49.22 kyr to 1.873 m.y. In higher-order solutions, variations in (e,ϖ) become coupled to variations in (I,Ω), but the solutions can still be cast in terms of Poisson series like equations (2) and (3).

Laskar [4] has recently published a secular variation theory that is complete to fifth order in eccentricity and inclination. Agreement between this secular variation model and strictly numerical computations [5,6] is much better than for any previous analytical model. The inclination and eccentricity series for Earth and Mars each contain 80 distinct terms.

In computing these secular orbital variations, the Earth, Moon, and planets can all be treated as point masses. No internal structure or processes are relevant to orbital evolution. The physics of the process is simple and well understood, though development of proper mathematical tools to represent the long-term evolution remains an area of active research [4,6,7]. On the other hand, the rotational evolution does depend rather sensitively on various aspects of the structure and dynamics of the interior.

Lunar and solar gravitational torques acting on the oblate figure of the Earth cause the spin axis **s** to precess about the instantaneous orbit normal **n**. If the Earth is considered to be a rigid body, the evolution of the spin axis orientation is given by

$$d\mathbf{s}/dt = \alpha(\mathbf{n}\cdot\mathbf{s})(\mathbf{s}\times\mathbf{n}) \qquad (4)$$

where

$$\alpha = \frac{3(C-A)}{2Cn}\sum\frac{Gm_i}{b_i^3}\left\{1-3\sin^2(I_i)\right\} \qquad (5)$$

is a scalar rate factor that depends on intrinsic properties of the Earth, such as polar and equatorial moments of inertia (C,A) and rotation rate n, and on extrinsic influences, such as masses m, orbital inclinations I, and semiminor axes b, of the Moon and Sun. The solar and lunar torques together produce a precession of the spin axis of the Earth at a rate of $\alpha(\mathbf{n}\cdot\mathbf{s}) = 50.38$ arcsec/yr [8,9].

Unfortunately, in the case of Mars, the precession rate is still rather poorly known. The best estimates at present come from analysis of the Viking Lander range data, which yield values of 9.6 ± 0.6 arcsec/yr. Much smaller relative errors are frequently cited, but all such optimistic estimates are directly dependent upon an assumed value for the moment of inertia of Mars, which is highly model dependent [10], precisely because the axial precession rate is not known. The uncertainty in this parameter is the largest single impediment to accurate reconstructions of the obliquity history of Mars [11]. Fortunately, the Mars Observer mission radio science investigations will significantly improve our knowledge of the precession rate of Mars within a few months after orbit insertion.

Once the present spin axis direction s is known and orbital element histories are given via equations (2) and (3), an obliquity history can be constructed from equation (4) in two different ways. The linear perturbation approach [12–17] involves deriving coefficients of a trigonometric series, similar to equations (2) and (3), which yields the obliquity and longitude of perihelion directly as functions of time. An alternative is to apply standard numerical algorithms for solving initial value problems to generate a vector time series s(t) and then compute the obliquity and longitude of perihelion directly [11,18,19]. The spectrum of obliquity variations, in the linear perturbation model, is simply obtained from the inclination spectrum by shifting each frequency s_j by the lunisolar precession rate (a = 50.38 arcsec/yr for the Earth, or 8–10 arcsec/yr for Mars) and multiplying each amplitude N_j by the spectral admittance

$$F_j = \cos(\varepsilon)\left(\frac{s_j}{s_j - s}\right) \qquad (6)$$

There are several important features of this solution: (1) As a is positive, and s_j is negative in all cases, it is possible for the denominator to vanish; (2) near this resonance, the obliquity variations are large; and (3) at smaller or larger forcing frequencies, the obliquity variations are small.

Uncertainty in the obliquity history of Mars derives from two facts: the value of the precession rate is uncertain by 6% (compared to <0.04% for the Earth) and the obliquity history of Mars depends more sensitively on the precession rate than is the case for Earth because of a near resonance with some of the inclination forcing frequencies. To investigate the sensitivity of the computed martian obliquity history to assumed precession rate, a series of numerical integrations of the rigid body precession equations was made [11], covering a 20-m.y. interval centered on the present, using precession rates in the interval 8.5–9.5 arcsec/yr. The maximum obliquity encountered can be anywhere in the range 35°–50°, and the minimum value can be 8°–14°. Despite this large uncertainty in the particulars of the obliquity history, all the computed time series were characterized by two dominant features: large oscillation with a characteristic period of $\sim 10^5$ yr and a significant modulation with a characteristic period of $2\ 10^6$ yr.

Fourier, Legendre, and Milankovitch: The influence of orbital and rotational variations on climate is operative through perturbations in the latitudinal and seasonal pattern of insolation. The diurnal average intensity of radiation at a point is inversely proportional to the squared solar distance and directly proportional to the diurnal average rectified solar direction cosine

$$F = (a/r)^2 \langle \| u \cdot u_s \| \rangle \quad (7)$$

where a and r are mean and instantaneous solar distance, and u and u_s are unit vectors from the center of the Earth to the surface point of interest and the subsolar point respectively. The insolation pattern, as a function of latitude θ and mean anomaly M, can be readily computed once values are specified for the orbital and rotational parameters ε, e, and ϖ [14,15,18,20,21]. This pattern can also be written in terms of a Fourier-Legendre series [20,22–24]

$$F(\mu, M; \varepsilon, e, \varpi) = \sum P_n(\mu) \sum \exp(ipM)\, F_{n,p}(\varepsilon, e, \varpi) \quad (8)$$

where $\mu = \cos(\theta)$ and P_n is a Legendre polynomial. The number of terms in the Fourier summation required to obtain a good representation of the seasonal pattern is greater in the polar regions than in the tropics and mid latitudes. The primary difficulty in the polar regions is reproducing the abrupt change in slope of the insolation curve at times of transition to continual darkness or continual light. It is also true that the polar regions place the greatest demands on the Legendre summation, since the spatial pattern also has a discontinuous first derivative at the latitude where the transition occurs to continual darkness or light.

Precessional Dynamics with Variable Rate: All but the most recent reconstructions of the radiative forcing input to paleoclimate models have assumed that both the orbital and rotational dynamics could be readily and accurately reconstructed from their present configurations via the simple analyses mentioned in the introduction. These expectations seem well founded in the case of orbital evolution, though the possibility of chaotic dynamics in the inner solar system [7,25] does seem to preclude confident extrapolation beyond 10^7 yr. However, there are a number of processes, working in different locations and at different rates, that all serve to compound the difficulty of accurately computing the spin precessional evolution .

On the longest timescales of interest (10^7–10^9 yr) the limiting uncertainty is variability in the tidal transfer of angular momentum from the rotation of the Earth to the orbit of the Moon. At present, these tidal torques are increasing the length of the day by 22.5 10^{-6} s/yr and increasing the size of the lunar orbit by 3.88 cm/yr [26,27]. Berger et al. [28] have made a useful first step toward including this effect in climatic time series. They computed the change in the major precession and obliquity frequencies due to lunar tidal evolution assuming that the present rate of tidal energy dissipation is representative of the past 500 m.y. However, the present rates are considerably higher than the long-term average [29], largely due to a near resonance between sloshing modes of ocean basins and the diurnal and semidiurnal tidal periods [30], and apparently compounded by a contribution from shallow seas [31,32]. Sedimentary records that constrain lunar orbital evolution show some promise of resolving this problem [33–36], but the situation is definitely more complex than is suggested by Berger et al. [28].

Another parameter that can vary, on rather shorter timescales and in an equally irregular fashion, is the gravitational oblateness of the Earth (C-A)/C. Thomson [37] has recently made three important contributions to the understanding of this source of variability. First, he pointed out that mass redistribution associated with major glaciations and compensating subsidence and crustal deformations [38,39] can cause fractional changes in oblateness of order 10^{-3}–10^{-2}. Second, he showed that high-resolution spectral analyses of several climatic time series appear to indicate fluctuations of the lunisolar precession rate of this magnitude, and with a dominant period near 100 kyr. Finally, Thomson pointed out that the best fit to the paleoclimate proxy data was obtained using a mean lunisolar precession rate 0.6 arcsec/yr less than the present observed value. He notes that the resulting value would correspond rather closely with that expected for a hydrostatic flattening [40]. If these important results are corroborated, they will demonstrate that important feedback loops exist in the orbital-rotational-climatic interactions system, further "up-stream" in the presumed causal chain than has been previously recognized.

Differential Precession of the Mantle and Core: The hydrostatic figure of a planet represents a compromise between gravitation, which attempts to attain spherical symmetry, and rotation, which prefers cylindrical symmetry. Due to its higher mean density, the core of the Earth is more nearly spherical than the mantle. The direct lunisolar precessional torques on the core will thus be inadequate to make it precess at the same rate as the mantle. In fact, the core oblateness is only about three-fourths that required for coprecession with the mantle [41]. However, it is clearly the case that the core and mantle precess at very nearly the same rate [42]. A variety of different physical mechanisms contributes to the torques that achieve this coupling, but a purely phenomenological partitioning is useful. The net torque can be described as a sum of inertial torques, which are parallel to $(\chi_m \times \chi_c)$, and dissipative torques, which are parallel to $(\chi_m - \chi_c)$. Here, χ_c and χ_m are the rotation vectors of the core and mantle respectively. The two types of torques have qualitatively different results: Inertial torques cause the core and mantle axes to precess at fixed angular separations and on the opposite side of their combined angular momentum vector,

whereas the effect of dissipative torques is to reduce the angle between the axes.

On short timescales it is appropriate to consider the core to be an inviscid fluid constrained to move within the ellipsoidal region bounded by the rigid mantle [43–45]. The inertial coupling provided by this mechanism is effective whenever the ellipticity of the container exceeds the ratio of the precessional to rotational rates. If the mantle were actually rigid, or even elastic [46,47], this would be an extremely effective type of coupling. However, on sufficiently long timescales, the mantle will deform viscously and can accommodate the motions of the core fluid [48]. The inertial coupling torque exerted by the core on the mantle will have the form

$$T_i = k_i[\chi_m \times \chi_c] \tag{9}$$

A fundamentally different type of coupling is provided by electromagnetic or viscous torques [49–51]. The dissipative coupling torque exerted by the core on the mantle will have the form

$$T_d = k_d[\chi_m \times \chi_c] \tag{10}$$

This type of coupling is likely to be most important on longer timescales. In each case, the mantle exerts an equal and opposite torque on the core. The response of the coupled core-mantle system to orbital forcing is given by [52–54]

$$\begin{aligned} ds_m/dt &= \alpha_m(n \cdot s_m)(s_m \times n) - \beta_m(s_m - s_c) - \gamma_m(s_m \times s_c) \\ ds_c/dt &= \alpha_c(n \cdot s_c)(s_c \times n) + \beta_c(s_m - s_c) + \gamma_c(s_m \times s_c) \end{aligned} \tag{11}$$

where α_m is similar to α above, except that only mantle moments A_m and C_m are included, and

$$\begin{aligned} \beta_m &= k_d/C_m\upsilon \\ \gamma_m &= k_i/C_m\upsilon^2 \end{aligned} \tag{12}$$

where υ is the mean rotation rate.

References: [1] Hays T. D. et al. (1976) *Science, 194,* 1121–1132. [2] Berger A. L. et al. (1984) *Milankovitch and Climate,* Reidel, Dordrecht, 895 pp. [3] Milani A. (1988) In *Long-term Dynamical Behavior of Natural and Artificial N-body Systems* (A. E. Roy, ed.), 73–108, Reidel, Boston. [4] Laskar J. (1988) *Astron. Astrophys., 198,* 341–362. [5] Richardson D. L. and Walker C. F. (1989) *J. Astron. Sci., 37,* 159–182. [6] Quinn T. R. et al. (1991) *Astron J., 101,* 2287–2305. [7] Laskar J. (1990) *Icarus, 88,* 266–291. [8] Kinoshita H. (1977) *Celest. Mech., 15,* 215–241. [9] Williams K. G. et al. (1991) *Astron. Astrophys., 241,* L9–L12. [10] Bills B. G. (1989) *GRL, 16,* 385–388. [11] Bills B. G. (1990) *JGR, 95,* 14137–14153. [12] Miskovic V. V. (1931) *Glas. Spr. Kral'yevske Acad., 143.* [13] Sharaf S. G. and Boudnikova N. A. (1967) *Bull. Inst. Theor. Astronon., 11,* 231–261. [14] Vernekar A. D. (1972) *Meteor. Mon., 12,* 1–22. [15] Vernekar A. D. (1977) In *The Solar Output and Its Variations* (O. R. White, ed.), 117–130, Univ. of Colorado. [16] Ward W. R. (1974) *JGR, 79,* 3375–3381. [17] Berger A. L. (1976) *Astron. Astrophys., 51,* 127–135. [18] Ward W. R. (1979) *JGR, 84,* 237–241. [19] Laskar J. (1986) *Astron. Astrophys., 157,* 59–70. [20] Hargreaves R. (1895) *Trans. Camb. Phil. Soc., 16,* 58–94. [21] Milankovitch M. (1920) *Theorie Mathématique des Phenomènes Thermiques Produits par la Radiation Solaire,* Gauthier-Villars, Paris, 336 pp. [22] North G. R. and Coakley J. A. (1979) *J. Atmos. Sci., 36,* 1189–1204. [23] Taylor K. E. (1984) In *Milankoitch and Climate* (A. L. Berger et al., eds.), 113–125, Reidel, Dordrecht. [24] Bills B. G. (1992) *Clim. Dynam.,* submitted. [25] Laskar J. et al. (1992) *Icarus, 95,* 148–152. [26] Cazenave A. and Daillet S. (1981) *JGR, 86,* 1659–1663. [27] Christodoulidis D. C. et al. (1988) *JGR, 93,* 6216–6236. [28] Berger et al. (1989) *Paleocean, 4,* 555–564. [29] Hansen K. S. (1982) *Rev. Geophys. Space Phys., 20,* 457–480. [30] Platzman G. W. et al. (1981) *J. Phys. Ocean., 11,* 579–603. [32] Dickman S. R. and Preisig J. R. (1986) *Geophys. J., 87,* 295–304. [33] Olsen P. E. (1986) *Science, 234,* 842–848. [34] Williams G. E. (1989) *J. Geol. Soc. London, 146,* 97–111. [35] Williams G. E. (1989) *Eos, 70,* 33–41. [36] Herbert T. D. and D'Hondt S. L. (1990) *EPSL, 99,* 263–275. [37] Thomson D. J. (1990) *Trans. R. Soc. Lond., A332,* 539–597. [38] Le Treut H. and Ghil M. (1983) *JGR, 88,* 5167–5190. [39] Wu P. and Peltier W. R. (1984) *Geophys. J., 76,* 753–791. [40] Nakiboglu S. M. (1982) *PEPI, 28,* 302–311. [41] Smith M. L. and Dahlen A. F. (1981) *Geophys. J., 64,* 223–281. [42] Stacey F. D. (1973) *Geophys. J.,* 33, 47–55. [43] Poincare H. (1910) *Bull. Astron., 27,* 322–356. [44] Toomre A. (1966) In *The Earth-Moon System,* 33–45, Plenum. [45] Voorhies C. V. (1991) *J. Geomag. Geoelec., 43,* 131–156. [46] Merriam J. B. (1988) *PEPI, 50,* 280–290. [47] Smylie D. E. et al. (1990) *Geophys. J. Int., 100,* 183–192. [48] Wu P. (1990) *Geophys. J. Int., 101,* 213–231. [49] Rochester M. G. (1962) *JGR, 67,* 4833–4836. [50] Sasao T. et al. (1977) *Publ. Astron. Soc. Japan, 29,* 83–105. [51] Kubo Y. (1979) *Celest. Mech., 19,* 215–241. [52] Goldreich P. and Peale S. J. (1970) *Astron. J., 75,* 273–284. [53] Ward W. R. and DeCampli W. M. (1979) *Astrophys. J. Lett., 230,* 117–121. [54] Bills B. G. (1990) *LPSC XXI,* 81–82.

CONDENSATION PHASE OF THE MARTIAN SOUTH POLAR CAP.

J. Capuano, M. Reed, and P. B. James, Department of Physics and Astronomy, University of Toledo, Toledo OH 43606, USA.

One type of database that can be useful in constraining models of the martian surface-atmosphere system is the time-dependent boundary of CO_2 frost for the polar caps. These

data have the advantage of spanning a large number of annual cycles on the planet, although, because a large fraction of the coverage is Earth based, the resolution for interannual comparisons is somewhat limited.

A more significant problem with these data is that they are almost exclusively obtained during the spring-summer recessions of the two polar caps. There are good reasons for this heavy weighting toward the sublimation phases, especially in the telescopic data. The martian poles are tilted away from the Sun, and therefore from Earth, between the fall and spring equinoxes. The presumed edge of the polar cap during fall and winter therefore barely extends past the terminator, where the resolution is degraded both by geometry and by the martian atmosphere. An additional complication is clouds, especially in the north polar region where the edge of the cap is obscured by the polar hood throughout most of the deposition seasons. The same lighting and obscuration problems are also a problem for spacecraft observations, though to a much smaller degree; however, there are few observations of the fall-winter caps in the set of spacecraft observations.

Data acquired by thermal infrared sensors on spacecraft are not constrained by the lighting problems that hamper visual observations. The surface temperature of solid CO_2 is constrained by Clapeyron's Equation as a function of the local partial pressure of CO_2 gas. The latter depends on the elevation, scale height, and total amount of CO_2 that is condensed in both polar regions; however, the temperature varies relatively slowly with pressure and, assuming that the surface temperature for polar CO_2 deposits is constant at some T between 147 and 150 K, is a valid first approximation. The infrared data are, however, potentially susceptible to deviations of the frost from blackbody conditions as well as to optically thick clouds, which can suppress the observed temperature through scattering.

We have investigated the growth of the martian south polar cap using the Viking IRTM dataset, which is available on the Atmospheres Node of the Planetary Data System in Boulder, Colorado. These data are available in five bands, four of which should correspond to surface radiation in clear conditions; we have chosen to work with the 20-μm data in the first phases of the project. The data are binned in 2° latitude and longitude intervals, in 10° intervals of areocentric solar longitude, L_s, and in 4-hr intervals of the local time of day at which the observations were made. We chose here to average over the local time variable; this is justified by the fact that many of the models do not include diurnal effects in predicting cap edges and by the fact that the diurnal effects should be small compared to the bin size. The effects of this averaging will be considered at a later time. We have also divided the data into three longitude bins: 1–45, 170–220, and 300–345. These were chosen because the extensive Viking dataset pertaining to south polar regression shows very different temporal and spatial behaviors in these three regions [1]. It is hoped that some correlation with the behavior during condensation may be found to help explain the large south polar cap asymmetry.

The major deficiency of these data is that they are binned in 10° L_s increments so that the temporal resolution is not very desirable. In addition, there are no data for some of the regions of interest in some of these time bins. However, we have been able to extract "curves of growth" for the three cap wedges mentioned above, which are shown in Fig. 1. There are some anomalous time periods in particular regions in which the "curves of growth" appear to be discontinuous; the most obvious one occurs between 330° and 45° longitude and between L_s = 45 and 55. This anomalous behavior shows up in all the wavelength bands that will respond to the lower atmosphere and surface, so it therefore seems likely that this is a real effect rather than a data problem. The most likely explanation for such excursions appears to be that clouds near the edge of the cap are affecting the measured brightness temperatures by scattering the infrared radiation emitted by the surface; if the effect were due to a reduced emissivity for fresh CO_2 deposits it would be more likely to show up more often in the data. Clouds were identified as a likely mechanism for the very low temperatures observed in the polar regions during the Viking Mission [2] and are predicted by GCM simulations [3] under some conditions. After L_s = 200° the data points show the effects of dust storms on Mars that commenced at L_s = 205° and cannot be used straightforwardly.

The data points from early autumn define a relatively smooth "curve of growth" for the cap that seems to be consistent with the limited visual data available. There is some suggestion of a lag in cap growth between longitudes 170 and 220, which could be correlated with the early removal of frost in these regions during mid spring, though the statistical significance of the observed difference is not overwhelming. The peak in cap size seems to occur just before winter solstice, which is earlier than models suggest for the maximum

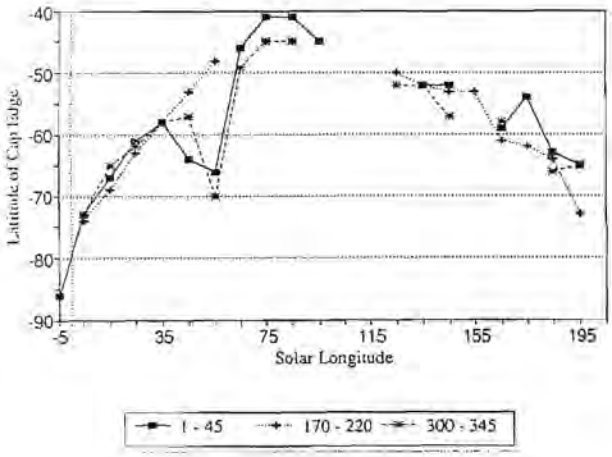

Fig. 1. South polar ice cap.

extent. It is possible that these bins could be dominated by data from the Argyre and Hellas Basins, which are within the two longitude wedges represented at these times; further study of the data in these L_s bins will be needed to resolve this question.

Acknowledgments: This work was partially supported by the NASA Planetary Atmospheres Program through Grant NAGW 2337.

References: [1] James P. B. et al. (1979) *JGR, 84,* 2889–2922. [2] Kieffer H. H. et al. (1976) *Science, 193,* 780–786. [3] Pollack J. B. et al. (1990) *JGR, 95,* 1447–1474.

WATER ON MARS: INVENTORY, DISTRIBUTION, AND POSSIBLE SOURCES OF POLAR ICE. S. M. Clifford, Lunar and Planetary Institute, 3600 Bay Area Blvd., Houston TX 77058, USA.

Theoretical considerations and various lines of morphologic evidence suggest that, in addition to the normal seasonal and climatic exchange of H_2O that occurs between the martian polar caps, atmosphere, and mid- to high-latitude regolith (e.g., [1,2]), large volumes of water have been introduced into the planet's long-term hydrologic cycle by the sublimation of equatorial ground ice, impacts, catastrophic flooding, and volcanism. Under the climatic conditions that are thought to have prevailed on Mars throughout the past 3–4 b.y., much of this water is expected to have been cold-trapped at the poles. In this abstract the amount of polar ice contributed by each of the planet's potential crustal sources is discussed and estimated. The final analysis suggests that only 5–15% of this potential inventory is now in residence at the poles.

Recent estimates of the inventory of water on Mars suggest that the planet has outgassed the equivalent of a global ocean at least several hundred meters deep. Evidence for such a large inventory is provided by a long list of martian landforms whose morphology has been attributed to the existence of subsurface volatiles [3–6]. In particular, it is supported by the existence of the martian outflow channels, whose distribution, size, and range of ages suggest that a significant body of groundwater was present on Mars throughout much of its geologic history [4,5,7,8]. Based on a conservative estimate of the discharge required to erode the channels, and the likely extent of their original source region, Carr [4,5] estimates that Mars may have outgassed the equivalent of a global ocean of water 0.5–1 km deep.

On Mars there are essentially three reservoirs in which water can reside: the atmosphere, perrenial polar caps, and near-surface crust. Of these, the atmosphere is known to contain ~15 precipitable micrometers of water averaged over the planet's surface, while the quantity of water stored as ice in the polar caps is equivalent to a global layer approximately 10 m deep. This leaves more than 98% of the suspected global inventory of water on Mars unaccounted for—virtually all of which is thought to reside as ground ice and groundwater beneath the surface.

Although mean annual surface temperatures are below freezing everywhere on Mars, observations made by the Viking Orbiter Mars Atmospheric Water Detectors (MAWD) indicate a globally averaged frost point temperature of ~198 K. Therefore, given the present latitudinal range of mean annual surface temperatures (~154–218 K), any subsurface H_2O is unstable with respect to the water vapor content of the atmosphere at latitudes equatorward of ±40° [9].

The survival of ground ice at equatorial and temperate latitudes was considered in detail by both Clifford and Hillel [10] and Fanale et al. [11]. They found that, for reasonable values of porosity and pore size, the near-equatorial crust has probably been desiccated to a depth of 300–500 m over the past 3.5 b.y., assuming that our present knowledge of the quasiperiodic changes in martian obliquity and orbital elements is accurate (e.g., [12–14]. However, because the sublimation of H_2O is sensitively dependent on temperature, the quantity of ice lost from the regolith is expected to decline with increasing latitude, falling to perhaps a few tens of meters at a latitude of 35° [10,11].

By integrating the the likely pore volume between the martian surface and the desiccation depths discussed above, Fanale et al. [11] have estimated that over the course of martian geologic history as much as 2.7–5.6 × 10^6 km^3 of H_2O (equivalent to a global ocean ~20–40 m deep) may have been sublimed from the equatorial regolith and cold-trapped at the poles. However, as mentioned at the outset of this discussion, the sublimation of equatorial ground ice is just one of several potential processes that may have episodically introduced large volumes of water into the atmosphere.

Perhaps the clearest evidence that the martian crust has been a major source of atmospheric water are the outflow channels. The abrupt emergence of these features from regions of collapsed and disrupted terrain suggests that they were formed by a massive and catastrophic release of groundwater [7,8,15]. Channel ages, inferred from the density of superposed craters, indicate at least several episodes of flooding—the oldest dating back as far as the Late Hesperian (~2–3 b.y. ago), while the youngest may have formed as recently as the Mid-to-Late Amazonian (i.e., within the last 1 b.y.) [16–20]. Based on a conservative estimate of how much material was eroded to form the channels (~5 × 10^6 km^3) and the maximum sediment load that the flood waters could have carried (40% by volume), Carr [5] has estimated a minimum cumulative channel discharge of 7.5 × 10^6 km^3 of H_2O (the equivalent of a global ocean ~50 m deep).

Impacts into the ice-rich crust may have been another important source of atmospheric water. Assuming that the thickness of permafrost on Mars averages about 2.5 km and has an ice content of 20%, the volume of water excavated

and/or volatilized by an individual impact will range from ~34 km^3 for a crater 10 km in diameter to in excess of 2.8 × 10^5 km^3 for a major impact basin like Hellas (D ~ 2000 km). Given a global crater size-frequency distribution equivalent to that preserved in the cratered highlands (e.g., [21]), the resulting total volume of water that may have been injected into the atmosphere by impacts over the course of martian geologic history is roughly 1.5 × 10^7 km^3 (~105 m). Note that, because the crater statistics of [21] do not include any correction for obliteration or erosion, this estimate is likely a lower bound.

Finally, as discussed by Greeley [22] and Plescia and Crisp [23], volcanism has probably also introduced large volumes of water into the martian atmosphere. For example, if the water content of martian magmas is comparable to that of terrestrial mafic to ultramafic lavas (~1% by weight), Plescia and Crisp [23] estimate that the formation of the volcanic plains in southeastern Elysium (5°N, 195°W) may have alone exsolved between 10^3–10^4 km^3 of H_2O. Greeley [22] has taken a more global perspective, calculating the total volume of juvenile water released from the planet's interior by estimating the extent and thickness of all volcanic units visible on the planet's surface. However, the estimate of extrusive magma production on which Greeley's [22] calculation is based has recently been revised by Greeley and Schneid [24]. Substituting this revised figure into Greeley's [22] analysis suggests that volcanic processes have injected ~2.3 × 10^6 km^3 (~16 m) of H_2O into the atmosphere. It should be noted, however, that in light of our inability to accurately assess both the extent of plutonic activity and the magnitude of ancient (>4 b.y. old) volcanism, this estimate is probably a minimum. Note also that, unlike water derived from other crustal sources (which simply undergoes an exchange from one volatile reservoir to another), water released by volcanism represents an actual addition to the planet's outgassed inventory of H_2O. However, once this water has been introduced into the atmosphere, its fate is governed by the same processes that affect water derived from any other crustal source—leading to a slow but inexorable transfer of water from equatorial and temperate latitudes to the poles [10,11].

Indeed, even if we consider only those sources of atmospheric H_2O for which there is unambiguous evidence (i.e., volcanism and catastrophic floods), it suggests that Mars should possess a polar inventory of H_2O roughly an order of magnitude greater (~1 × 10^7 km^3) than that which is presently observed in the caps. If the potential contribution from impacts and the sublimation of equatorial ground ice is also included, it could easily increase this disparity by an additional factor of three.

Potential solutions to this mass balance problem include (1) the amount of water released to the atmosphere by volcanism, catastrophic floods, and other processes may have been significantly smaller than presently believed; (2) the geographic location of the spin axis of Mars has wandered over geologic time due to changes in the planet's moment of inertia, thereby redistributing ice cold-trapped at the poles over a much larger area of the planet [25]; or (3) the bulk of the ice deposited in the polar regions has been reintroduced into the crust through the process of basal melting [26]. A more detailed discussion of polar deposition, basal melting, and the polar mass balance is contained in Clifford [27].

References: [1] Jakosky B. (1985) *Space Sci. Rev., 41,* 131–200. [2] Zent A. P. et al. (1986) *Icarus, 67,* 19–36. [3] Rossbacher L. A. and. Judson S. (1981) *Icarus, 45,* 39–59. [4] Carr M. H. (1986) *Icarus, 68,* 187–216. [5] Carr M. H. (1987) *Nature, 326,* 30–35. [6] Squyres S. (1989) *Icarus, 79,* 229–288. [7] Sharp R. P. and Malin M. (1975) *GSA Bull., 86,* 593–609. [8] Baker V. (1982)*The Channels of Mars,* Univ. of Texas, Austin. [9] Farmer C. B. and Doms P. E. (1979) *JGR, 84,* 2881–2888. [10] Clifford S. M. and Hillel D. (1983) *JGR, 88,* 2456–2474. [11] Fanale F. P. et al. (1986) *Icarus, 67,* 1–18. [12] Ward W. (1979) *JGR, 84,* 237–241. [13] Toon O. B. et al. (1980) *Icarus, 44,* 552–607. [14] Bills B. G. (1990) *JGR, 95,* 14137–14153. [15] Carr M. H. (1979) *JGR, 84,* 2995–3007. [16] Neukum G. and Wise D. (1976) *Science, 194,* 1381–1387. [17] Carr M. H. and Clow G. (1981) *Icarus, 48,* 91–117. [18] Tanaka K. (1986) *Proc. LPSC 17th,* in *JGR, 91,* E139–E158. [19] Parker T. J. et al. (1989) *Icarus, 82,* 111–145. [20] Rotto L. and Tanaka K. L. (1991) In *LPI Tech. Rpt. 92-02,* 111–112. [21] Barlow N. (1990) *JGR, 95,* 14191–14201. [22] Greeley R. (1987) *Science, 236,* 1653–1654. [23] Plescia J. B. and Crisp J. (1992) *LPI Tech. Rpt. 92-02,* 102–103. [24] Greeley R. and Schneid B. (1991) *LPS XXII,* 489–490. [25] Schultz P. H. (1985) *Sci. Am., 253,* 94–102. [26] Clifford S. M. (1987) *JGR, 92,* 9135–9152. [27] Clifford S. M. (1992) *JGR,* submitted.

RHEOLOGY OF WATER-SILICATE MIXTURES AT LOW TEMPERATURES.

William B. Durham, Lawrence Livermore National Laboratory, Livermore CA 94550, USA.

Our laboratory studies of the effects of hard particulates on the rheology of ice have been mainly directed at the evolution of the Galilean satellites, but yield results that may be applicable to the rheology of the martian polar caps. Our experiments have explored the ductile rheology as well as brittle behavior of water + particulate (mainly quartz) mixtures in particulate volume fractions ϕ ranging from 0.001 to 0.56, particulate sizes 1–150 μm, temperatures 77–224 K, and deformation rates 3.5 × 10^{-7} to 3.5 × 10^{-4} s^{-1}, under confining pressures of 50–100 MPa. Particulates act mainly to strengthen the material in the ductile field, although work by others has shown that very close to the melting temperature hard particulates can actually cause softening (possibly by impeding grain growth). So-called dispersion hardening by

the Orowan mechanism of pinning glide dislocations, often exploited in metallurgy for strengthening materials, appears not to be an issue in ice except at very low temperatures, less than approximately 135 K. Significant hardening does appear in the ductile field at $\phi \geq 0.10$ and may be due to viscous drag in the ice matrix as it is forced to flow around the particulates. This effect is considerably greater than that expected from simple law-of-mixtures predictions. For $\phi = 0.10$ we measured an increase in viscosity of about 30%; the effect grows rapidly to a factor of 5 at $\phi = 0.30$ and a factor of 150 at $\phi = 0.60$. The proportional amount of strengthening is not strongly dependent on temperature over our measured range of 142–223 K. Microstructural studies suggest these results can vary. For example, we occasionally observe segregation of particles to intergranular regions, possibly swept there during periods of grain growth, effectively suppressing much of the viscous drag hardening.

In the brittle field, encountered at lower temperatures, lower confining pressures, and higher strain rates, the primary effect of particulate loading is a toughening: more work (not necessarily more stress) is required to produce the faulting instability. We suspect the cause is that particulates in the matrix act to limit crack growth, making a critical flaw length more difficult to achieve. The increased toughness manifests itself as a widening of the ductile field (at the expense of the brittle field) in parameter space. If there is any implication for martian glaciers, it is that near-surface fracturing will extend deeper in ice with lower particulate loads.

MARTIAN VOLATILES DETERMINED USING THE MARS OBSERVER GAMMA RAY SPECTROMETER.

W. C. Feldman[1], W. V. Boynton[2], J. I. Trombka[3], J. R. Arnold[4], P. A. J. Englert[5], A. E. Metzger[6], R. C. Reedy[1], S. W. Squyres[7], and H. Wänke[8], [1]Los Alamos National Laboratory, Los Alamos NM, USA, [2]Lunar and Planetary Laboratory, University of Arizona, Tucson AZ, USA, [3]NASA Goddard Space Flight Center, Greenbelt MD, USA, [4]Department of Chemistry, University of California–San Diego, La Jolla CA, USA, [5]Department of Chemistry, San Jose State University, San Jose CA, USA, [6]Jet Propulsion Laboratory, Pasadena CA, USA, [7]Center for Radiophysics and Space Research, Cornell University, Ithaca NY, USA, [8]Max-Planck-Institut für Chemie, Mainz, Germany.

The relative abundances of H_2O and CO_2 and their latitude, longitude, and depth profiles on Mars sensitively reflect, as well as help control, past and present martian climate patterns. Seasonal variations of their distributions at high latitudes also reflect and help control global weather patterns and erosion through surface weathering. A combined analysis of gamma ray line and neutron flux maps constructed from data measured using the Mars Observer Gamma Ray Spectrometer (MOGRS) should allow a determination of (1) seasonal changes in both the horizontal and vertical structure of CO_2 ice that covers the north polar cap during winter and the south polar cap throughout the year and (2) both the horizontal and vertical structure of residual H_2O ice within the top meter of the surface that was predicted from Viking observations to exist primarily at high latitudes. Particularly important in this regard will be maps of thermal and epithermal neutron fluxes measured using the forward- and backward-facing elements of the MOGRS anticoincidence shield, the intensity of the hydrogen, neutron-capture gamma ray line at 2.223 MeV, the intensity of a capture gamma ray line from a major element such as that at 1.725 MeV from iron, and the intensity of an inelastic scatter gamma ray line from a major element such as that at 1.779 MeV from silicon. Specific capabilities will be explored using computer simulations of expected MOGRS count rates in the Mars mapping orbit.

DO LARGE IMPACT BASINS IN THE SOUTHERN HEMISPHERE OF MARS CONTROL THE DISTRIBUTION OF POLAR STRUCTURES AND DEPOSITS?

Herbert Frey[1] and Anne-Marie Reidy[2], [1]Geodynamics Branch, Goddard Space Flight Center, Greenbelt MD 20771, USA, [2]Astronomy Program, University of Maryland, College Park MD 20742, USA.

Introduction: Among the outstanding problems in martian geology are the cause of the off-axis and asymmetric distribution of the southern polar layered terrain and residual ice deposits and the cause of the orientation of scarps, valleys, and reentrant canyons that occur there. A perhaps related problem region is the apparently small number of large (D > 500 km) impact basins seen in the relatively well-preserved cratered terrain of the south polar region. Previously only the 850-km-wide South Polar Basin was easily recognized [1–4]. We have been mapping the south polar region in detail, searching for evidence of ancient, highly degraded impact basins, which may have escaped earlier notice, for two reasons: To determine (1) whether the apparent absence of large impact basins is due to incomplete mapping and recognition or a fundamental characteristic of the martian crust related to the origin of the martian crustal dichotomy [5,6] and (2) whether ancient impact basins, if they exist, exert some control on the distribution of volcanic and polar deposits in the southern hemisphere and on the topography on which these deposits lie. We previously described [7] several promising candidates, including a large pre-Hellas basin in the Malea Planum region and an older but comparably sized basin overlapping South Polar [8,9]. In this paper we concentrate on the possible influence of the candidate basins in localizing the asymmetric distribution of polar deposits and in controlling the orientation of structures found within these deposits.

We search for evidence of concentric distribution of relict scarps, massifs, dissected ancient terrain, indicators of subsurface structure (changes in orientation of channels, offsets in in faults or linear featruin faults or linear features), and in faults or linear features), and direct indicators of low topography (elevation data, valley networks, runoff channels, localized plains deposits), and focus the search by assuming that any unrecognized large impact basin must be nearly buried, and its area may be depopulated in large impact craters. Impact basins may be good traps for volcanic, aeolian, and polar deposits, all of which (if thick enough) may have obscured later-forming large craters. Alternatively, late formation of a large basin may have eliminated earlier large craters.

Candidate Basins in the South Polar Region: We earlier identified large (>1000 km across), roughly circular regions that appear deficient in the population of craters larger than 100 to 150 km [7,8]. The Malea Planum region shows some structural evidence for a large impact basin, centered at about 328°W, 68°S [8,9]. There is structural evidence for three rings (diameters 620 km, 1020 km, and 1680 km), including concentric distribution of ridges, highly degraded blocks of Noachian terrain much like massifs around Argyre, and arclike occurrences of knobby terrain. Three other possible rings (diameters ~800 km, 1370 km, and 2100 km) are less well marked. The basin is overlapped by outer rings of the Hellas Basin; together the two may explain the Hesperian-age ridged plains volcanism that overlies the southern rim of Hellas [8] and forms Malea Planum.

There is very good structural evidence for a smaller overlapping basin (Malea B) to the southwest, centered closer to the pole at about 340°W, 75°S, near the fresh crater South. Two reasonably well-defined but incomplete rings, marked by massifs, isolated peaks, and outcrops of knobby and degraded Noachian terrain bounded by scarps, have diameters 545 km and 810 km. Evidence for two possible outer rings (diameters 1065 km and 1245 km) is weaker, but the *influence* of Malea B may extend even further, to over 1000 km from the center of the basin (see below). Overlap of this smaller basin with the proposed Malea Basin confines most of the polar plains unit *Hdu* in the Sisyphus region, and overlap with South Polar Basin appears related to the distribution of polar ice and perhaps the layered terrain deposits (see below).

South Polar Basin is the most obvious impact basin in the southern polar region, but its single recognized ring—the disjointed scarplike Promethei Rupes—is unusual. It is impossible to fit all the segments of the exposed scarp with a single circular arc. We suggest that influence from other basins, including Malea B, South Polar B (see below), and even the distant but larger Hellas Basin, has affected the structure of the South Polar rim. As in the case of Malea B, the distribution of ridged plains, outcrops of ancient terrain, ridges, scarps, and other features suggests the *influence* of South Polar Basin greatly exceeds its variable 850–900-km diameter. We found rare individual peaks, scarps, and some ridges in spotty, sometimes concentric distribution at distances of 350 km, 590 km, 811 km, and 1000 km about the center of South Polar Basin, which might mark rings at 700 km, 1180 km, 1622 km, and 2000 km. Better imaging and topographic data from Mars Observer may help to determine whether or not South Polar Basin is truly a multiring structure.

Evidence exists for an overlapping basin we call South Polar B [9]. A variety of features including straightened crater rims, a subtle 45-km-long scarp, a 200-km-long knobby ridge, a group of massifs and mountainous peaks, a 300-km-long concentric ridge, an inward-facing, 85-km-long scarp 505 km from the center, and a series of short ridges, scattered knobs, and small massifs all suggest a partially buried ring 1010 km wide centered at 206°W, 73°S. A possible second ring (D ~ 1375 km) is suggested by a break in the rim of South Polar Basin, deflection of an 85-km northwest trending ridge, a 50-km-long straightened crater rim, small (10–20 km long) sinuous but concentric ridges, a small 10-km-long massif, and similar features.

The 1000-km diameter of the most prominant (middle?) ring makes South Polar B slightly larger than South Polar, but its highly degraded state and obvious overprinting by the Promethei Rupes suggest it formed earlier.

Influence of Large Basins on Polar Structures and Deposits: We previously described how the overlap of the proposed Malea Basin with outer rings of Hellas may have controlled the location of the ridged plains (*Nplr* and *Hr*) in Malea Planum. It also appears that the location and overlap of Malea B, South Polar, and South Polar B control the location of important polar terrain units. Nearly all the *Hdu* and *Hdl* units in the eastern portion of the south polar region lie within the Malea B and South Polar Basins. Likewise, the polar layered terrain (*Apl*) appears to lie mostly within South Polar and South Polar B (Fig. 1), even though there is no obvious rim preserved on the northwestern edge of the unit. It may be that by itself South Polar cannot account for the localization of the layered terrain units, but the basin certainly appears to have played a role. We also note that the extended distribution of *Apl* northward about 180°W longitude appears directly related to the overlap between South Polar and South Polar B (Fig. 1).

The off-axis location of the residual ice deposits (*Api*) is more difficult to explain, being located far from the center of South Polar B and only lying within overlap of the more distant Malea B rings with South Polar. The *Api* units are located at the approximate center of a large, roughly circular region in which large craters are nearly absent. Perhaps there remains to be found a very ancient basin whose overlap with South Polar and Malea B provides the proper topographic trap not only for *Apl* units but for *Api* as well. A basin centered at 85°W, 78°S in the Cavi Agusti region would not only

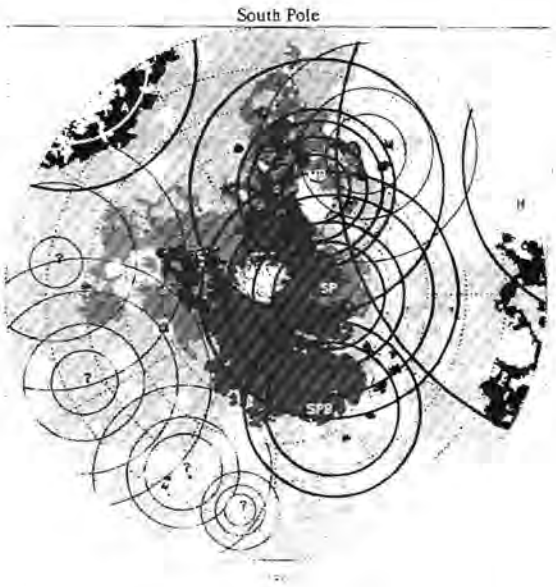

Fig. 1. Candidate large impact basins in the south polar region. Of particular interest are Malea B (MB), South Polar (SP), and South Polar B (SPB), which may have some control over the distribution of polar layered terrain (*Apl*) and other polar deposits (*Hdl*, *Hdu*). Also shown for reference are Argyre (A), Hellas (H), and Malea (M), as well as several much less certain candidates for which there is only weak and indirect evidence (?). Note the polar layered terrain (*Apl*, shown as dark gray) lies within the extended influence of South Polar Basin, as inferred from concentrically distributed structures. Chasma Australe lies on an arc concentric to Malea B that also seems to control narrow valleys in the residual ice terrain (*Api*, white inside dark gray), a distorted rim of a large crater near the Dorsa Argentea, and several very long ridges in Malea Planum (see text for details).

provide the proper overlap but also help explain the distribution of *Hdu* and *Hdl* units in the western south polar region and many of the structures found there. With improved imsible to determine whether there remains any vestige of such possible ancient structures.

Malea B, South Polar, and South Polar B may play a role in the orientation of structures (scarps, valleys, Chasma Australe) within the layered terrains. Many of these occur along the orientation of proposed rings of these basins, as arcs concentric to basin centers, or along lines radial to a basin center (sometimes where combinations of these conditions exist). Malea B appears to be particularly important in this regard. Ridges in the *Nplr* and *Hr* units of Malea Planum, as well as valleys and scarps in the layered terrain *Apl*, all lie on arcs concentric to the Malea B center. The bounding sides of the major reentrant Chasma Australe lie along two broad arcs concentric about the center of Malea B, which also appears to control several of the narrow valleys within *Api*, mark the boundary between cratered terrain and *Nplr* ridged plains that run northward from South Polar Basin rim between 280° and 290°W, and lie along several prominant ridges with Malea Planum. Several long valleys within the residual ice *Api* are oriented toward the center of either South Polar or South Polar B; shorter cross-cutting valleys in the same unit seem more aligned with the center of Malea B. Within the layered terrain away from the residual ice deposits, several long ridges at about 150°W are also radially oriented toward South Polar B. By contrast, the prominant facing scarps at 300°W, 85°S are not so obviously associated with any of these basins, and may reflect still additional influences not yet recognized.

While not explaining everything seen in the south polar region, there is convincing but at the present only circumstantial evidence that the three basins described above did exert substantial influence on the distribution of polar deposits (*Hdu*, *Hdl*, *Apl*, *Api*) and on the orientation of many of the structures found within these deposits. Both radial and concentric directions appear important, and in many places the combination of these from different basins may have contributed to the localization of structures.

References: [1] Schultz R. A. and Frey H. V. (1990) *JGR, 95,* 14175–14189. [2] Pike R. J. and Spudis P. D. (1987) *Earth Moon Planets, 39,* 129–194. [3] Croft S. K. (1981) *Proc. LPS 12B,* 277–257. [4] Wood C. A. and Head J. W. (1976) *Proc. LSC 7th,* 3629–3651. [5] Frey H. and Schultz R. A. (1990) *JGR, 95,* 14203–14213. [6] Frey H. (1991) *LPSC XXII,* 417–418. [7] Frey H. et al. (1991) *LPSC XXII,* 419–420. [8] Frey H. et al. (1991) *LPSC XXII,* 421–422. [9] Reidy A. M. et al. (1992) *LPSC XXIII,* 1137–1138.

EVOLUTION OF THE MARTIAN ATMOSPHERE: THE ROLE OF THE POLAR CAPS.

R. M. Haberle, D. Tyler, C. P. McKay, and W. Davis, NASA/Ames Research Center, Moffett Field CA 94035-1000, USA.

Several lines of evidence indicate that early in its history Mars had a much thicker CO_2 atmosphere than it does today. Pollack et al. [1] suggest that as much as 5 bar of CO_2 may have been in the atmosphere 4.5 b.y. ago. More recently, Kasting [2] has shown that without additional greenhouse gases in the atmosphere, CO_2 will condense (in the atmosphere), and that this will limit the amount it can hold. For the early martian environment, when the solar luminosity was 70% of its present value, this constraint leads to a 1.5-bar upper limit on the atmospheric abundance of CO_2. However, if Mars did begin with as much as 5 bar of CO_2 (assuming there were additional greenhouse gases), then where is it now? The present martian atmosphere contains only 7 mbar of CO_2. The main reservoirs for the rest of the initial CO_2 are the regolith, the polar caps, and carbonate rocks. The size of the regolith and rock reservoirs is uncertain; the cap reservoir appears to be small, perhaps several millibars.

We have constructed a model for the evolution of the martian atmosphere that self-consistently calculates the rates at which CO_2 is stored in these various reservoirs. Given some

initial abundance, which is assumed to be entirely in the atmosphere, the model calculates the annually averaged temperature of the equatorial region and the polar region, and the planetwide mean. This calculation is based on the model of Gierasch and Toon [3], which we have modified to include a greenhouse effect. CO_2 is then weathered out of the atmosphere using the temperature and pressure-dependent parameterization of Pollack et al. [1] and McKay and Davis [4]. What remains in the atmosphere is then partitioned between the regolith and caps assuming the regolith can hold 300 mbar at present conditions (215 K, 7 mbar). The model then repeats these steps at 90-m.y. intervals, increasing the solar luminosity linearly to its present value.

Thus far we have obtained results for the case where CO_2 condensation in the atmosphere is not a limiting factor. The results fall into two categories: initial inventories above 1 bar and initial inventories below 1 bar. For initial inventories above 1 bar, CO_2 is immediately partitioned between the atmosphere and regolith with the latter taking up almost 800 mbar of CO_2. The rest remains in the atmosphere and is weathered out at a rate proportional to atmospheric pressure. Eventually, the atmospheric pressure becomes low enough (~100 mbar) that heat transport into the polar regions is no longer able to prevent polar caps from forming. At that point, the climate system collapses: atmospheric pressure drops catastrophically (to several millibars), huge polar caps form (~500 mbar), and the regolith gives up its CO_2 and equilibrates to about 300 mbar. The higher the initial pressure, the later in time this event occurs. For a 5-bar initial abundance the collapse occurs at 2 b.y.; for a 1-bar initial abundance the collapse occurs much earlier at around 700 m.y. For the remainder of the simulation, the caps slowly give up their CO_2 to the regolith and atmosphere, but they never disappear.

For initial inventories less than 1 bar, the evolution scenario is different. In these cases, polar caps form immediately since there is not enough greenhouse warming to prevent CO_2 from going into the regolith and thereby reducing the atmospheric pressure to levels where caps can form. In a sense, these simulations begin with a collapsed climate system. As the Sun brightens and temperatures warm, the caps shrink, giving up their CO_2 to the atmosphere, regolith, and rock reservoirs. Interestingly, these low initial abundance simulations suggest that the (permanent) polar caps are on the verge of disappearing at the present time.

While the results obtained thus far are intriguing, we cannot favor or rule out any particular scenario. However, it is clear that the evolution of the martian atmosphere may not have been monotonic in time, and that this result is directly attributable to the formation of polar caps. As was pointed out by Leighton and Murray [5] in 1966, once permanent polar caps form on Mars, their heat balance determines the surface pressure.

References: [1] Pollack J. B. et al. (1987) *Icarus, 71,* 203–224. [2] Kasting J. F. (1991) *Icarus, 94,* 1–13. [3] Gierasch P. J. and Toon O. B. J. (1973) *Atmos. Sci., 30,* 1502–1508. [4] McKay C. P. and Davis W. L. (1991) *Icarus, 90,* 214–221. [5] Leighton R. B. and Murray B. C. (1966) *Science, 153,* 136–144.

THE POLAR LAYERED DEPOSITS ON MARS: INFERENCES FROM THERMAL INERTIA MODELING AND GEOLOGIC STUDIES.

K. E. Herkenhoff, Geology and Planetology Section, Jet Propulsion Laboratory, California Institute of Technology, Pasadena CA 91109, USA.

It is widely believed that the martian polar layered deposits record climate variations over at least the last 10–100 m.y. [1–8], but the details of the processes involved and their relative roles in layer formation and evolution remain obscure [9]. A common presumption among Mars researchers is that the layered deposits are the result of variations in the proportions of dust and water ice deposited over many climate cycles [3–5], but their composition is poorly constrained [10]. The polar layered deposits appear to be the source of dark, saltating material that has been distributed over the surface of Mars [11], but the mechanisms by which this material is incorporated and eroded from the layered deposits are unknown. These mechanisms must be understood before the processes that formed and modified the layered deposits can be inferred and related to martian climate changes.

Calculations of the stability of water ice in the polar regions of Mars [5,12] indicate that ice is not currently stable at the surface of the layered deposits. The present water-ice sublimation rate is high enough to erode the entire thickness of the deposits in about a million years. This result suggests that sublimation of water ice from the layered deposits results in concentration of nonvolatile material at the surface of the deposits. Such a surface layer would insulate underlying water ice from further sublimation, stabilizing the layered deposits against rapid erosion. The low albedo of the layered deposits does not necessarily indicate that an insulating dust layer is present, as the observed albedo only constrains the fraction of dust at the surface to be greater than 0.1% by mass if mixed with water-ice grains that have radii of 0.1 mm or larger [13]. The existence of a surface layer is more strongly supported by the low apparent thermal inertia of the surface of the south polar layered deposits [14]. However, a similar mapping study of the north polar region indicates that water ice is present near the surface of the north polar layered deposits and subliming into the atmosphere [15]. Hence, it appears that while the present erosion rate of the south polar layered deposits is low, the north polar layered deposits (at least in some areas) are currently being eroded by ice sublimation. These inferences have important implications for the present water budget on Mars, and for the recent climate history of the planet.

The color and albedo of the layered deposits suggest that bright, red dust is the major nonvolatile component of the deposits. I have constructed a new Viking Orbiter 2 color mosaic of part of the south polar region, taken during orbit 358, using controlled images provided by T. Becker of the U.S. Geological Survey in Flagstaff. Analysis of this color mosaic indicates that a bright, red unit extends beyond the layered deposits, supporting my previous interpretation of this unit as mantling dust [16,17]. This result also supports the inference that the layered deposits contain both bright and dark materials in addition to water ice. The differences in albedo and color between mantling dust and exposures of layered deposits and the association of dark saltating material indicates that there is at least a minor component of dark material in the deposits [11,16]. If the dark material is composed of solid sand-sized grains, poleward circulation is required to transport the sand (by saltation) into the layered deposits [18]. Saltating sand would eject dust into suspension, hindering codeposition of sand and dust. However, sand may have saltated over ice-cemented dust toward the poles at some previous time when winds blew onto the polar caps. In this case, the dark sand must have formed layers or lenses less than a few meters in size, or they would be visible in high-resolution Viking Orbiter images. Alternatively, dark dust (rather than sand) may be intimately mixed with bright dust in the layered deposits.

How can dark dust in the layered deposits form the dunes observed in the polar regions? Sublimation of dust/ice mixtures has been shown to result in the formation of filamentary sublimation residue (FSR) particles of various sizes [19]. Such particles can saltate along the martian surface, and may therefore create dunes [20,21]. In order to form saltating material that is at least three times darker (in red light) than the bright dust that mantles much of Mars, dark dust grains must preferentially form FSR particles. Magnetic dust grains would be expected to form FSR more easily than nonmagnetic dust, and are probably much darker. Experimental formation of FSR with magnetic material has not been attempted, and should be the subject of future research.

There is direct evidence for 1–7% magnetic material (magnetite or maghemite) in the surface fines at the Viking lander sites [22]. In addition, analysis of Viking lander sky brightness data indicates that suspended dust over the landing sites contains about 1% opaque phase, perhaps of the same composition as the magnetic material on the surface [22,23]. Within the uncertainties in these measurements, the percentages of magnetic material given above are identical to the volume of dark dune deposits in the polar regions expressed as a percentage of the estimated volume of eroded layered deposits [18,24]. This comparison indicates that the presence of magnetic dust in the layered deposits is likely, and that formation of dunes from dark FSR particles is plausible. Eventual destruction of the particles could allow recycling of the dark dust into the layered deposits via atmospheric suspension. Under the assumption that FSR can be formed by sublimation of mixtures of water ice and magnetic dust, the thermal properties of this material have been estimated and compared with observational data, as detailed below.

A recent study using Viking IRTM observations of an area completely covered by dunes within the north polar erg [24] shows that the dunes have thermal inertias of less than 100 J m^{-2} $s^{-1/2}$ K^{-1} [15]. Previous interpretations of martian thermal inertia data in terms of particle sizes have utilized the relationship between these quantities presented by Kieffer et al. [25], which is based primarily upon measurements of the thermal properties of quartz sands [26]. The low albedos of martian dunes are inconsistent with a siliceous composition, so basalt grains and magnetite FSR are considered here. The thermal conductivities of the materials considered here are only weakly dependent on temperature between 200 and 300 K, so values measured near 300 K have been used in all cases.

The thermal conductivity of basaltic sands is about 1.2 × 10^{-2} W m^{-1} K^{-1} (~40%) less than that of pure quartz sands of the same size (~100 μm). If the polar dunes are composed purely of basaltic grains, their effective particle size is no greater than about 50 μm (40% porosity). Particles in this size range will be transported by atmospheric suspension [27], and are therefore not likely to form dunes. Hence, low-inertia materials that are capable of saltation must be examined as possible dune-forming materials on Mars. The thermal properties of FSR particles are therefore estimated below.

The density of magnetite is 5200 kg m^{-3}, almost twice that of quartz (2650 kg m^{-3}) or basalt (2680–2830 kg m^{-3}). The specific heat of magnetite is 544 J kg^{-1} K^{-1} at 220 K [28], only slightly less than the specific heat of various silicates [29]. The porosity of clay FSR formed in laboratory experiments is 99% [19]. Magnetite FSR would therefore have a bulk density of only 52 kg m^{-3}. The thermal conductivity of porous clay at 313 K, 740 torr ranges from 0.477 to 2.05 W m^{-1} K^{-1}, depending on water content [28]. The lowest value is identical to that of clay FSR [19]. When this dry clay was placed in a high vacuum, its thermal conductivity decreased only 7%. Therefore, the conductivity of clay FSR at 6 mbar is probably no greater than 0.47 W m^{-1} K^{-1}. The thermal conductivity of clay minerals is probably similar to that of most silicates, about 2.8 times less than the conductivity of magnetite. Hence, magnetite FSR should have a thermal conductivity of 1.2 W m^{-1} K^{-1} or less, implying a thermal inertia of no more than 187 J m^{-2} $s^{-1/2}$ K^{-1}. The thermal inertia of ensembles of FSR particles may be lower still, and is compatible with the north polar erg thermal inertias derived from Viking data.

In summary, weathering of the martian layered deposits by sublimation of water ice can account for the thermal inertias, water vapor abundances, and geologic relationships observed in the martian polar regions. The nonvolatile component of

the layered deposits appears to consist mainly of bright red dust, with small amounts of dark dust. Dark dust, perhaps similar to the magnetic material found at the Viking Lander sites, may preferentially form filamentary residue particles upon weathering of the deposits. Once eroded, these particles may saltate to form the dark dunes found in both polar regions. This scenario for the origin and evolution of the dark material within the polar layered deposits is consistent with the available imaging and thermal data. Further experimental measurements of the thermophysical properties of magnetite and maghemite under martian conditions are needed to better test this hypothesis.

References: [1] Murray B. C. (1972) *Icarus, 17,* 328–345. [2] Cutts J. A. et al. (1976) *Science, 194,* 1329–1337. [3] Cutts J. A. et al. (1979) *JGR, 84,* 2975–2994. [4] Squyres S. W. (1979) *Icarus, 40,* 244–261. [5] Toon O. B. et al. (1980) *Icarus, 44,* 552–607. [6] Carr M. H. (1982) *Icarus, 50,* 129–139. [7] Howard A. D. et al. (1982) *Icarus, 50,* 161–215. [8] Plaut J. J. et al. (1988) *Icarus, 76,* 357–377. [9] Thomas P. et al. (1992) In *Mars*, Univ. of Arizona, Tucson, in press. [10] Malin M. C. (1986) *GRL, 13,* 444–447. [11] Thomas P. C. and Weitz C. (1989) *Icarus, 81,* 185–215. [12] Hofstadter M. D. and Murray B. C. (1990) *Icarus, 84,* 352–361. [13] Kieffer H. H. (1990) *JGR, 95,* 1481–1493. [14] Paige D. A. and Keegan K. D. (1992) *JGR,* submitted. [15] Paige D. A. et al. (1992) *JGR,* submitted. [16] Herkenhoff K. E. and Murray B. C. (1990) *JGR, 95,* 1343–1358. [17] Herkenhoff K. E. and Murray B. C. (1992) *U.S. Geol. Surv. Misc. Inv. Ser. Map I-2304,* in press. [18] Thomas P. (1982) *JGR, 87,* 9999–10008. [19] Storrs A. D. et al. (1988) *Icarus, 76,* 493–512. [20] Saunders R. S. et al. (1985) *NASA TM-87563,* 300–302. [21] Saunders R. S. and Blewett D. T. (1987) *Astron. Vestnik, 21,* 181–188. [22] Hargraves R. B. et al. (1979) *JGR, 84,* 8379–8384. [23] Pollack J. B. et al. (1979) *JGR, 84,* 4479–4496. [24] Lancaster N. and Greeley R. (1991) *JGR, 95,* 10921–10927. [25] Kieffer H. H. et al. (1973) *JGR, 78,* 4291–4312. [26] Wechsler A. E. and Glaser P. E. (1965) *Icarus, 4,* 335–352. [27] Edgett K. S. and Christensen P. R. (1991) *JGR, 96,* 22765–22776. [28] Touloukian Y. S. et al. (1970) In *Thermophysical Properties of Matter,* Vols. 2 and 5, IFI/Plenum, New York. [29] Winter D. F. and Saari J. M. (1969) *Astrophys. J., 156,* 1135–1151.

THE MARS WATER CYCLE AT OTHER EPOCHS: RECENT HISTORY OF THE POLAR CAPS AND LAYERED TERRAIN.

Bruce M. Jakosky, Bradley G. Henderson, and Michael T. Mellon, Laboratory for Atmospheric and Space Physics, University of Colorado, Boulder CO 80309-0392, USA.

The martian polar caps and layered terrain presumably evolve by the deposition and removal of small amounts of water and dust each year; the current cap attributes therefore represent the incremental transport during a single year as integrated over long periods of time. We have investigated the role of condensation and sublimation of water ice in this process by examining the seasonal water cycle during the last 10^7 yr. In our model, axial obliquity, eccentricity, and L_s of perihelion vary according to dynamical models. At each epoch we calculate the seasonal variations in temperature at the two poles, keeping track of the seasonal CO_2 cap and the summertime sublimation of water vapor into the atmosphere; net exchange of water between the two caps is calculated based on the difference in the summertime sublimation between the two caps (or on the sublimation from one cap if the other is covered with CO_2 frost all year). Despite the simple nature of our model and the tremendous complexity of the martian climate system, our results suggest two significant conclusions: (1) Only a relatively small amount of water vapor actually cycles between the poles on these timescales, such that it is to some extent the same water molecules moving back and forth between the two caps. (2) The difference in elevation between the two caps results in different seasonal behavior, such that there is a net transport of water from south to north averaged over long timescales. These results can help explain (1) the apparent inconsistency between the timescales inferred for layer formation and the much older crater retention age of the cap and (2) the difference in sizes of the two residual caps, with the south being smaller than the north.

POSSIBLE RECENT AND ANCIENT GLACIAL ICE FLOW IN THE SOUTH POLAR REGION OF MARS.

J. S. Kargel, U.S. Geological Survey, 2255 N. Gemini Drive, Flagstaff AZ, USA.

Martian polar science began almost as soon as small telescopes were trained on the planet. The seasonal expansion and contraction of the polar caps and their high albedos led most astronomers to think that water ice is the dominant constituent. In 1911 Lowell [1] perceived a bluish band around the retreating edge of the polar caps, and he interpreted it as water from melting polar ice and seasonal snow. An alternative idea in Lowell's time was that the polar caps consist of frozen carbonic acid. Lowell rejected the carbonic acid hypothesis primarily on account of his blue band. To complete his refutation, Lowell pointed out that carbonic acid would sublimate rather than melt at confining pressures near and below one bar; hence, carbonic acid could not account for the blue watery band. Some of the many ironies in comparing Lowell's theories with today's knowledge are that we now recognize that (1) sublimation is mainly responsible for the growth and contraction of Mars' polar caps, (2) carbon dioxide is a major component of the southern polar cap, and (3) Lowell's blue band was probably seasonal dust and/or clouds.

Melting of water ice certainly is not a significant extant polar process.

It has been eight decades since Lowell [1] discussed the composition of Mars' polar caps, and considered the roles of glaciers (moving ice) and seasonal snow or frost (static ice) as contributors to the polar caps. Although we now have a far better observational base to consider these matters, and have made considerable progress in understanding the polar caps, these basic issues remain largely unresolved.

This abstract presents geomorphic evidence that glacial ice and glacial melt waters once flowed over broad areas of the southern polar region. Earlier reports by the author and co-workers have suggested similar processes and associated hydrologic phenomena across many other areas of the martian surface [2,3]. Two aspects of the south polar region suggest possible glacial processes during two distinct eras in Mars' history. First, the lobate marginal form of polar layered deposits is consistent with geologically recent glacial flow; this is considered weak evidence because purely sublimational processes might produce the same structure. Stronger evidence, in the writer's view, is the observation that landforms in regions surrounding the polar layered deposits seem to bear the imprint of ancient but far more extensive glacial processes. Some geomorphologic evidence is presented below.

The great sinuous ridges of Dorsa Argentea and nearby "etched plains" in the south polar region (Figs. 1 and 2) were interpreted by Howard [4] as having formed by basal melting of ground ice. He thought that the ridges may have formed by deposition of fluvial sediment between large blocks of ground ice. If the ice had been active at some time (i.e., moving), such features would be termed *kame moraines,* a truly glacial landform. However, it seems that Howard had in mind more static bodies of ice-rich soil or rock that would not be considered glacial. Howard [4] also considered a more strictly glacial interpretation that the ridges of Dorsa Argentea are eskers, but he did not favor this hypothesis on account of a perceived absence of associated glacial landforms.

Kargel and Strom [3,5,6] have examined the glacial esker model for the formation of Dorsa Argentea and similar sinuous ridges elsewhere on Mars. They found that terrestrial eskers bear many geomorphic aspects in common with martian sinuous ridges, and, furthermore, identified a host of associated landforms that are plausibly explained by glaciation. Other researchers also have explored the possible genesis of sinuous ridges on Mars [7–13]. All these workers have considered glacial esker or eskerlike hypotheses as acceptable purely on the basis of the characteristics of the ridges. However, every group of researchers has come to a different conclusion concerning what they "probably" are! Proposed analogues include longitudinal sand dunes, inverted stream beds, lacustrine spits or bars, clastic dikes, wrinkle ridges, igneous dikes, and volcanic flows, in addition to the eskers favored here. On the basis of present data it would be fruitless for anyone to try to prove one model to the exclusion of others. This abstract simply shows that other glacial-appearing features do exist in the southern polar region of Mars in association with Dorsa Argentea.

Figure 2 shows part of Dorsa Argentea adjacent to an area of higher ground. The high ground exhibits many elongate depressions, including some in a conspicuous radial pattern. Generally, these depressions are sharp-edged pits 10 to 100 km long and several hundred meters deep (based on shadow measurements). This terrain is part of the south polar etched terrain, which is generally regarded as the result of either (1) eolian deflation or (2) sublimation or melting of massive ground ice. A third hypothesis is that these depressions were eroded by active glacial ice and melt water. In this case, they would be roughly analogous in scale, form,

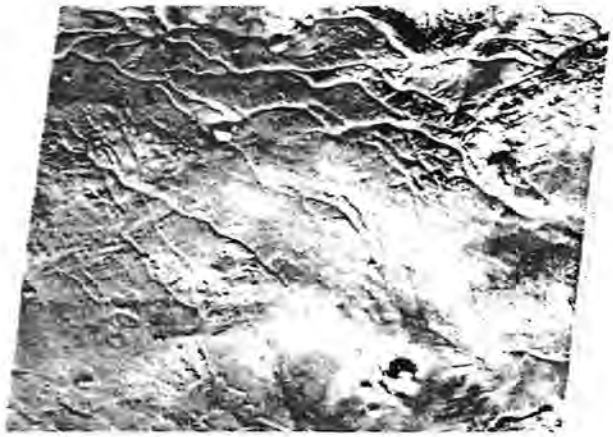

Fig. 1. Part of Dorsa Argentea, near latitude 78°S, longitude 40°. Scene width 213 km. Solar illumination from top 12° above horizon. VO image 421B53.

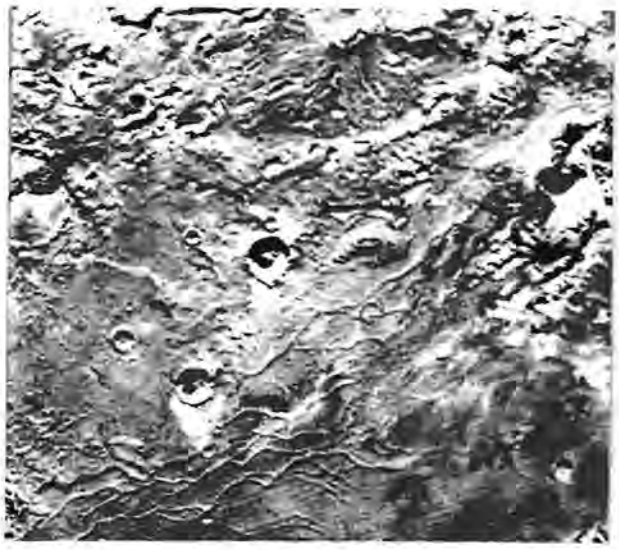

Fig. 2. Another view of Dorsa Argentea, showing also adjoining areas of etched terrain near latitude 76°S, longitude 30°. Solar illumination from top. Scene width 357 km. VO 421B16.

and origin to the fjord lakes of British Columbia and Scotland and the finger lakes of New York. Some of these terrestrial features, such as the New York finger lakes, tend to have smoothly rounded edges, while others, including many of the fjord lakes of British Columbia and Scotland, have fairly sharp edges. All of these terrestrial features were eroded by glacial ice streams and catastrophic glacial melt water releases late in the Pleistocene when climatic amelioration destabilized the continental ice sheets.

Figure 3 shows an area roughly 400 km southeast of the nearest parts of Dorsa Argentea. The rugged area near the center of the image is one of the highest regions in the southern hemisphere of Mars. The scalloped form of the mountains is similar to terrestrial mountain ranges modified by alpine glaciation. The scalloped embayments, some compound, resemble terrestrial glacial cirques and glacial valleys. Figure 4 is a Landsat image of the Sentinel Range, Antarctica, seen at a resolution similar to the Viking scene. The Sentinel Mountains are dominated by simple and compound cirques ("cirque-in-cirque" structure). The Mars scene exhibits a similar morphology. The smooth plains in the Mars scene and the smooth glacial ice sheet in Antarctica both possess faint lineations streaming away from the mountains. In the Antarctic scene (Fig. 4) the lineations are lateral and medial moraines and pressure ridges in the ice closely approximate glacial flow lines. While one cannot prove it with present data, thoroughly moraine-mantled glacial ice with glacial flow lines or ground moraine retaining former ice-flow structures are reasonable interpretations of the Mars scene (Fig. 3). A working hypothesis is that the high mountains in Fig. 3 served as a major source of ice ultimately responsible for the formation of the Dorsa Argentea ridges. Another source may have been the etched plains to the northeast of Dorsa Argentea (Fig. 2).

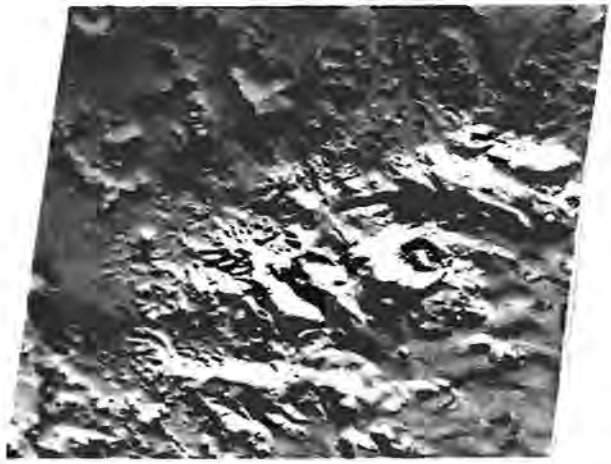

Fig. 3. Mountainous region and adjoining lineated plains ~400 km southeast of Dorsa Argentea, near latitude 81°S, longitude 347°. Solar illumination from top. Scene width 172 km. VO 421B83.

Fig. 4. Landsat image of Sentinel Mountains, Antarctica. Solar illumination from top. Scene width ~200 km. Courtesy of Baerbel Lucchitta and the Flagstaff Image Processing Facility, U.S. Geological Survey.

Mars Observer will have the capabilities to address the glacial and competing hypotheses. For instance, glacial erratics, if they exist, should be visible in narrow-angle images as randomly distributed bright spots one to several pixels wide with long shadows. These images may reveal abundant moraines, some containing resolvable boulders, in some areas. Fluting, roches moutonnées, rock drumlins, and true drumlins should be readily visible on some glacially sculptured plains and alpine valleys. Narrow-angle images of eskers may reveal layering and cross-bedding and probably will show thermokarstic features. Images of ice-sculptured basins should show small-scale sculptural forms such as fluting and roches moutonnées and may reveal glaciolacustrine deltas and eskers. Mars Observer infrared observations of plains containing many eskers and covered by ground moraines should indicate abundant gravel-, cobble-, and boulder-sized material, while thermal infrared data for large glacial lake plains should indicate mainly very fine-grained sediment. Laser altimetry should reveal characteristic U-shaped transverse profiles of many glacial valleys. In combination with imagery, laser altimetry may indicate ice-flow directions opposing the topographic gradient of the rock surface in some cases and may indicate longitudinal gradient reversals of eskers.

References: [1] Lowell P. (1911) *Mars and Its Canals*, Macmillan, New York, 393 pp. [2] Baker V. R. et al. (1991) *Nature, 352*, 589–594. [3] Kargel J. S. and Strom R. G. (1992) *Geology, 20*, 3–7. [4] Howard A. D. (1981) *NASA TM-84211*, 286–288. [5] Kargel J. S. and Strom R.G. (1990)

LPSC XXI, 598–599. [6] Kargel J. S. and Strom R. G. (1991) *LPSC XXII*, 683–684. [7] Carr M. H. (1984) In *The Geology of the Terrestrial Planets* (M. H. Carr, ed.), 231–232, NASA SP-469. [8] Parker T. J. et al. (1986) *NASA TM-88383*, 468–470. [9] Parker T. J. and Gorsline D. S. (1992) *LPSC XXIII*, 1031–1032. [10] Tanaka K. L. and Scott D. H. (1987) *Geologic Map of the Polar Regions of Mars*, U.S. Geol. Surv. Misc. Inv. Ser. Map I-1802-C. [11] Ruff S. W. and Greeley R. (1990) *LPSC XXI*, 1047–1048. [12] Metzger S. M. (1991) *LPSC XXII*, 891–892. [13] Metzger S. M. (1992) *LPSC XXIII*, 901–902.

IS CO_2 ICE PERMANENT? Bernhard Lee Lindner, Atmospheric and Environmental Research, Inc., 840 Memorial Drive, Cambridge MA 02139, USA.

Carbon dioxide ice has been inferred to exist at the south pole in summertime [1,2], but Earth-based measurements in 1969 of water vapor in the martian atmosphere suggest that all CO_2 ice sublimed from the southern polar cap and exposed underlying water ice [3]. This implies that the observed summertime CO_2 ice is of recent origin.

However, Fig. 1 shows that theoretical models of the energy budget of the surface that simulate the formation and dissipation of CO_2 ice have been unable to preserve seasonal CO_2 ice at the south pole and still obtain agreement with observations of the polar cap regression and the annual cycle in atmospheric pressure [4–10]. This implies that either these models improperly treat the energy budget or that CO_2 ice from an earlier time is exposed in summer.

An exact comparison to data is difficult, considering that the edge of the polar cap is usually patchy and ill defined [18,19], in large part due to terrain that is not included in any polar cap model. The edge of the polar cap is also diurnally variable since ice frequently forms at night and sublimes during the day. There is also some year-to-year variability in polar cap regression [20,21].

Several processes have been examined that might retain the good agreement to observations of the annual cycle in atmospheric pressure and to overall polar cap regression, and yet allow for better agreement at the south pole, without requiring old CO_2 ice. The radiative effects of ozone were suggested as important [11], but were shown numerically to be unimportant [12,13]. However, the radiative effects of clouds and dust [12] and the dependence of frost albedo on solar zenith angle [14,15] do allow for better agreement at the pole while maintaining good agreement to overall polar cap regression and the atmospheric pressure cycle [16]. Penetration of sunlight through the seasonal ice also has a marginal positive effect on CO_2 ice stability at the pole itself because it allows some solar radiation that would otherwise sublime overlying CO_2 seasonal ice to sublime ice within the residual polar cap [17].

Figures 2 and 3 show my model predictions for polar cap regression compared to observations. Before solar longitude of 250°, south polar cap regression is predicted to be similar to that predicted by earlier models (compare to Fig. 1). However, the new model retains CO_2 ice year round at the

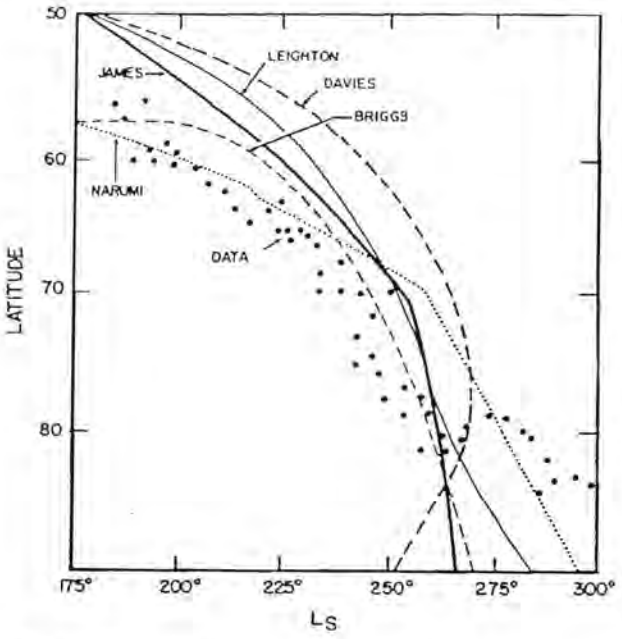

Fig. 1. The seasonal recession of the south polar cap as observed over the last 20 years [22] and as predicted by models [4,6–9]. (The aerocentric longitude of the Sun, L_s, is the seasonal index; L_s = 0°, 90°, 180°, and 270° correspond to northern spring equinox, summer solstice, autumnal equinox, and winter solstice respectively.)

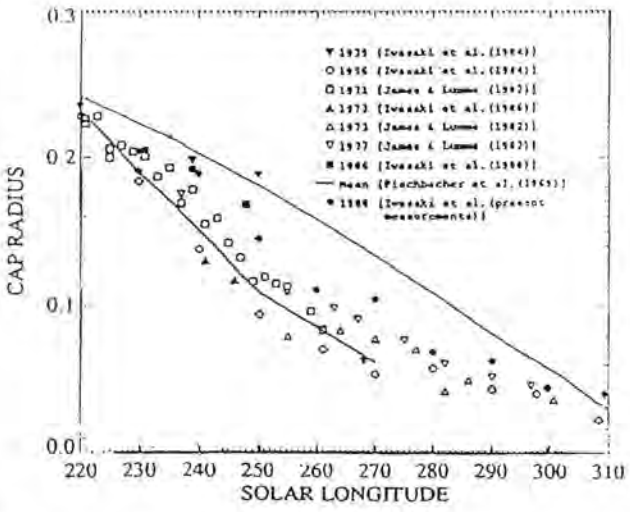

Fig. 2. The regression of the south polar cap, as observed for various years (taken from [23]) and as simulated by my model (thin line), as a function of the aerocentric longitude of the Sun (L_s). The cap radius is that which would be measured on a polar stereographic projection of the south polar region; the units of the radius are fractions of the planetary radius of Mars.

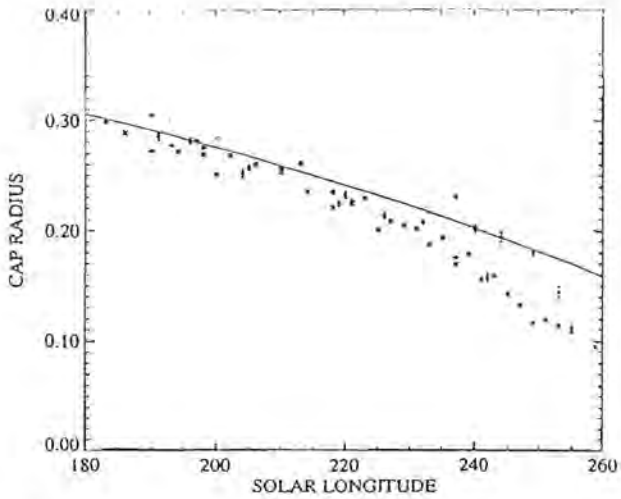

Fig. 3. The regression of the south polar cap, as observed in 1986 (solid circles), 1971 (crosses), and 1977 (plus signs) (taken from [21]) and as simulated by my model (thin line), as a function of the aerocentric longitude of the Sun (L_s). Two-sigma error bars are indicated for the 1986 data; the errors are smaller for the denser 1971 data and for the 1977 Viking data.

south pole. Unfortunately, the model does overpredict polar cap extent in early southern summer (see Fig. 2).

In summary, it appears possible to construct an energy balance model that maintains seasonal CO_2 ice at the south pole year round and still reasonably simulates the polar cap regression and atmospheric pressure data. This implies that the CO_2 ice observed in the summertime south polar cap could be seasonal in origin, and that minor changes in climate could cause CO_2 ice to completely vanish, as would appear to have happened in 1969 [3]. However, further research remains before it is certain whether the CO_2 ice observed in the summertime south polar cap is seasonal or is part of a permanent reservoir.

Acknowledgments. I acknowledge support by NASA contracts NASW 4444 and NASW 4614, under the Planetary Atmospheres Program and the Mars Data Analysis Program.

References: [1] Kieffer H. H. (1979) *JGR, 84,* 8263–8288. [2] Paige D. A. et al. (1990) *JGR, 95,* 1319–1335. [3] Jakosky B. M. and Barker E. S. (1984) *Icarus, 57,* 322–334. [4] Leighton R. B. and Murray B. C. (1966) *Science, 153,* 136–144. [5] Cross C. A. (1971) *Icarus, 15,* 110–114. [6] Briggs G. A. (1974) *Icarus, 23,* 167–191. [7] Davies D. W. et al. (1977) *JGR, 82,* 3815–3822. [8] Narumi Y. (1980) *Proceedings of the 13th Lunar and Planetary Symposium,* 31–41, Inst. Space Aeronaut. Sci., Univ. of Tokyo. [9] James P. B. and North G. R. (1982) *JGR, 87,* 10271–10283. [10] Lindner B. L. (1985) Ph.D. dissertation, Univ. of Colorado, Boulder, 470 pp. [11] Kuhn W. R. et al. (1979) *JGR, 84,* 8341–8342. [12] Lindner B. L. (1990) *JGR, 95,* 1367–1379. [13] Lindner B. L. (1991) *Icarus, 93,* 354–361. [14] Lindner B. L. (1991) In *International Union of Geodesy and Geophysics General Assembly XX, IAMAP Program and Abstracts,* 309, RM-Druck- and Verlagsgesellschaft, Graz, Austria. [15] Lindner B. L. (1992) In *Physics and Chemistry of Ice* (N. Maeno and T. Hondoh, eds.), 225–228, Hokkaido Univ., Sapporo. [16] Lindner B. L. (1992) *LPI Tech. Rpt. 92-02,* 76–77. [17] Lindner B. L. (1992) *GRL, 19,* 1675–1678. [18] Leovy C. B. et al. (1972) *Icarus, 17,* 373–393. [19] Christensen P. R. and Zurek R. W. (1983) *Bull. Am. Astron. Soc., 15,* 847. [20] Iwasaki K. et al. (1990) *JGR, 95,* 14751–14754. [21] James P. B. et al. (1990) *JGR, 95,* 1337–1341. [22] James P. B. and Lumme K. (1982) *Icarus, 50,* 368–380. [23] Iwasaki K. et al. (1990) *JGR, 95,* 14751–14754.

THE INTERANNUAL VARIABILITY OF POLAR CAP RECESSIONS AS A MEASURE OF MARTIAN CLIMATE AND WEATHER: USING EARTH-BASED DATA TO AUGMENT THE TIME LINE FOR THE MARS OBSERVER MAPPING MISSION.

L. J. Martin[1] and P. B. James[2], [1]Lowell Observatory, 1400 West Mars Hill Road, Flagstaff AZ 86001, USA, [2]Department of Physics and Astronomy, University of Toledo, Toledo OH 43606, USA.

Seasonal Cycles of Dust, Water, and CO_2: The recessions of the polar ice caps are the most visible and most studied indication of seasonal change on Mars. Strong, if circumstantial, evidence links these recessions to the seasonal cycles of CO_2, water, and dust. These phenomena and their interactions will be the subject of an MSATT workshop next year titled "Atmospheric Transport on Mars." Briggs and Leovy [1] have shown from Mariner 9 observations that the atmospheric polar hoods of the fall and winter seasons are at least partially water ice clouds. Around the time of the vernal equinox, this water ice may precipitate onto the surface that includes CO_2 frosts. The sublimation of the outer edge of the seasonal cap begins about this same time, and we begin to observe its recession. During the recession of the north cap we also observe cirumpolar clouds that are believed to be formed by water vapor from the subliming cap [2]. Some observations suggest that at least part of the sublimed water and/or CO_2 reforms as surface ice toward the cap's interior. This "new" ice is probably the bright component of the polar caps that is seen on Earth-based observations. This would explain the south cap's appearance as that of a shrinking donut during its recession [3]. Near the edge of the shrinking cap, dust activity is also evident on the Viking images [4]. This may result from off-cap winds generated from sublimation and/or dust that might be released from within or beneath the ices. It has been found that all of Mars' major dust storms that have been observed to date occurred during the broad seasons when either the north or south polar cap was receding [5]. There are short seasonal periods around the beginning and ending of cap recessions when no major dust

storms have been observed. Variable recession rates for the polar caps were suspected from Earth-based data and proven by Mariner 9 and Viking observations. The cycles for water, CO_2, and dust are thought to vary with the cap recessions, although the nature of the variations is not yet known. The possible relationship between variable recession rates and dust storm activity has been investigated by James et al. [6]. Iwasaki et al. [7] proposed a correlation between retarded cap recessions and the occurrence of major storms that seems plausible, although more data are needed. Certainly, the polar cap recession rates are at least one phenomenon that needs to be monitored in conjunction with dust storm activity. Since there is evidence that cap recessions may accelerate prior to the onset of encircling storms [5], this monitoring might even lead to predicting these storms. The possible advent of a planet-encircling storm during the Mars Observer (MO) Mission will provide a detailed correlation with a cap recession for that one martian year. We will then need to compare that cap recession with other storm and nonstorm years observed by other spacecraft and from Earth. MO data will also provide a stronger link between cap recessions and the water and CO_2 cycles. Cap recession variability might also be used to determine the variability of these cycles.

Observations—Present, Past, and Future: After nearly a century of valiant attempts at measuring polar cap recessions [8], including using Mariner 9 and Viking data [9–11], MO will provide the first comprehensive dataset. In contrast to MO, the older data are much less detailed and precise and could easily be forgotten, except that it will still be the only information on interannual variability. Since the MO mission will map just one martian year, it will provide a singular set of seasonal data. Standing alone it will not be possible to be certain which MO data are "seasonal" or whether an "average" or "abnormal" year is portrayed. Of course, even if MO could continue its work indefinitely, it might take a very long time to accumulate enough data to have a representative sample of Mars years. Therefore, we are obliged to retain and refer back to the still-viable historical records, including spacecraft data. These records will be easier to interpret and evaluate based upon new insights from MO data: By obtaining simultaneous Earth-based observations (including those from Hubble Space Telescope) during the MO mission, we will be able to make direct comparisons between the datasets. This will be very helpful in interpreting and measuring the Earth-based data taken during other periods. Continued Earth-based observations will be needed after MO to monitor the martian climate and extend the time line of the data. Improved techniques will allow us to monitor longer seasonal segments of martian years and to better interpret and measure the data. Eventually we may be able to establish limits on the degrees of variability of the polar cap recessions and, consequently, variations in the H_2O, CO_2, and dust cycles. Many of the questions presented by MO data and its upgraded portrayal of Mars can be addressed to longer-term, albeit cruder, Earth-based observations.

References: [1] Briggs G. A. and Leovy C. B. (1974) *Bull. Am. Met. Soc., 55,* 278. [2] James P. B. et al. (1987) *Icarus, 71,* 306. [3] Martin L. J. and James P. B. (1985) *LPI Tech. Rpt. 85-03,* 49. [4] Briggs G. A. et al. (1979) *JGR, 84,* 2795. [5] Martin L. J. and Zurek R. W. (1993) *JGR,* submitted. [6] James P. B. et al. (1987) *Icarus, 71,* 298. [7] Iwasaki K. et al. (1990) *JGR, 95,* 14751. [8] Martin L. J. et al. (1992) In *Mars* (H. Kieffer et al., eds.), Univ. of Arizona, Tucson, in press. [9] James P. B. et al. (1979) *JGR, 84,* 2889. [10] James P. B. (1979) *JGR, 84,* 8332. [11] James P. B. (1982) *Icarus, 52,* 565.

DUST TRANSPORT INTO MARTIAN POLAR LATITUDES. J. R. Murphy[1,2] and J. B. Pollack[2], [1]National Research Council Associate, [2]NASA Ames Research Center, Moffett Field CA 94035.

The presence of suspended dust in the martian atmosphere, and its ultimate return to the planet's surface, is implicated in the formation of the polar layered terrain and the dichotomy in perennial CO_2 polar cap retention in the two hemispheres. We have been employing a three-dimensional numerical model to study martian global dust storms. The model accounts for the interactive feedbacks between the atmospheric thermal and dynamical states and an evolving radiatively active suspended dust load. Results from dust storm experiments, as well as from simulations in which we are interested in identifying the conditions under which surface dust lifting occurs at various locations and times, indicate that dust transport due to atmospheric eddy motions is likely to be important in the arrival of suspended dust at polar latitudes.

The layered terrain in both the northern and southern polar regions of Mars is interpreted as the manifestation of cyclical episodes of volatile (CO_2, H_2O) and dust deposition. The cyclical nature of this deposition is assumed to be driven by long-period variations that arise from orbital and axial tilt variations and influence the climatic conditions. The dust is assumed to be provided primarily by the occurrence of global-scale dust storms that fill the atmosphere with large quantities of suspended dust, some of which settles back to the surface in the polar regions. The dust settles onto the cap either independently due to gravitational sedimentation or incorporated into CO_2 snow [1], possibly serving as condensation nuclei for such a process. The dust storms develop at southern subtropical latitudes, and barring any other sources (which is probably a poor assumption), the dust that appears in suspension at polar latitudes is transported over long distances. It has been a common belief that an intensified Hadley-type circulation is responsible for transporting the dust to high northern latitudes. However, two-dimensional

zonally symmetric numerical modeling of dust storms [2,3] has suggested that this mechanism is ineffective at transporting significant quantities of dust beyond middle latitudes. Recent three-dimensional numerical simulations conducted by us [4], in which the full spectrum of atmospheric eddy motions are present and capable of transporting dust, have shown that the amount of dust transported into polar regions from a southern subtropical source is greatly increased. The eddy transport mechanisms suggested in previous works [5,6] appear to be operating in these simulations.

The apparent preference for dust storm development during northern autumn and winter, when the north seasonal cap is growing, is interpreted as one reason for the retention of a perennial CO_2 residual cap in the south, while in the north all the CO_2 laid down during the winter season sublimes away in the spring. In the north, due to the dust incorporated into the cap during its growth, albedos during springtime are lower than the albedo of the south cap during its spring retreat, which develops during a typically less dusty time of the martian year [7,8]. The less "contaminated" south cap reflects more solar insulation, maintains a lower temperature during spring and summer, and thus is able to retain a cover of CO_2 ice throughout summer. In the north the lower cap albedo results in a larger net radiative flux at the cap surface and the CO_2 cap is unable to survive the summer.

We wish to point out that it is not necessarily the seasonal preference for dust storm development alone that conspires to affect the residual cap and layered terrain variations that are presently seen. Under present orbital characteristics, southern summer solstice occurs close in time to orbital perihelion, producing short "hot" summers and long cold winters in the south. This long cold winter results in a more extensive seasonal CO_2 cap in the south than in the north. The size of the cap can have implications for suspended dust reaching the pole, even in the absence of a global dust storm. Baroclinic waves, which develop due to the large horizontal temperature gradients at middle to high latitudes of the autumn, winter, and spring hemispheres, are probably capable of lifting dust from the surface. This lifted dust can then be carried poleward by these same waves. As the seasonal cap grows, the distance between the location of dust lifting and the pole increases, and thus the dust must be transported a greater distance if it is to become incorporated into the developing cap at polar latitudes, if in fact it can reach those latitudes [5]. Since the southern cap is, at its maximum extent, larger than the northern seasonal cap, the north cap (at polar latitudes) might be more susceptible to dust contamination than the south cap, even without dust storms. In fact, numerical simulations [9] suggest that the magnitude of baroclinic waves is larger in the north than in the south, further increasing the northern hemisphere preference for cap contamination by dust.

We will present model results detailing the mechanisms by which suspended dust is transported into polar latitudes and quantify polar dust deposition magnitudes as a function of various model assumptions.

References: [1] Pollack et al. (1979) *JGR, 84,* 2929–2945. [2] Haberle et al. (1982) *Icarus, 50,* 322–367. [3] Murphy et al. (1992) *JGR Planets,* submitted. [4] Murphy et al. (1992) in preparation. [5] Pollack J. B. and Toon O. B. (1980) *Icarus, 50,* 259–287. [6] Barnes J. B. (1990) *JGR, 95,* 1381–1400. [7] Colburn et al. (1989) *Icarus, 79,* 159–189. [8] Martin T. Z. (1986) *Icarus, 66,* 2–21. [9] Barnes et al. (1992) *JGR Planets,* submitted.

NUMERICAL SIMULATIONS OF DRAINAGE FLOWS ON MARS.

Thomas R. Parish[1] and Alan D. Howard[2], [1]Department of Atmospheric Science, University of Wyoming, Laramie WY 82071, USA, [2]Department of Environmental Sciences, University of Virginia, Charlottesville VA 22903, USA.

Introduction: Data collected by the Viking Landers (VL-1, 23°N; VL-2, 48 °N) have shown that the meteorology of the near-surface martian environment is analogous to desertlike terrestrial conditions [1]. Geological evidence such as dunes and frost streaks indicate that the surface wind is a potentially important factor in scouring of the martian landscape [2]. In particular, the north polar basin shows erosional features that suggest katabatic wind convergence into broad valleys near the margin of the polar cap. The pattern of katabatic wind drainage off the north polar cap is similar to that observed on Earth over Antarctica [3] or Greenland.

In this paper we will explore the sensitivity of martian drainage flows to variations in terrain slope and diurnal heating using a numerical modeling approach. The model used in this study is a two-dimensional sigma-coordinate primitive equation system [4] that has previously been used for simulations of Antarctic drainage flows. Prognostic equations include the flux forms of the horizontal scalar momentum equations, temperature, and continuity. Explicit parameterization of both longwave (terrestrial) and shortwave (solar) radiation is included [5]. Turbulent transfer of heat and momentum in the martian atmosphere remains uncertain since relevant measurements are essentially nonexistent. Standard terrestrial treatment of the boundary layer fluxes is employed [6–8].

Model Results: *Katabatic wind simulations.* A series of numerical experiments has been conducted that focuses on the relationship between katabatic wind intensity and terrain slope. The model runs are valid for high-latitude (75°), nocturnal conditions similar to midwinter on the north polar cap in which no solar radiation reaches the ground. A horizontal grid consisting of 20 points with a grid spacing of 20 km was used; 15 levels were used in the vertical with higher resolution in the lower atmosphere. The results of five uniform slope runs are presented here. Each model simulation covered

a 24-hr period; terrain slopes were set to 0.0005, 0.001, 0.002, 0.004, and 0.008. In each experiment, the model atmosphere was started from rest to isolate the katabatic wind. An initial lapse rate of 3°C km^{-1} was used with a surface temperature of approximately 220 K at the vertical reference level.

In all cases, the katabatic wind reached a quasisteady state within the first 12 hr. The resulting vertical profiles of wind speed and temperature for the five martian katabatic wind simulations after 24 hr are shown in Fig. 1. Curves A–E in this figure correspond to terrain slopes of 0.0005, 0.001, 0.002, 0.004, and 0.008 respectively. The intensity and depth of the katabatic wind (Fig. 1a) appear sensitive to the terrain slope. Note that despite the absence of ambient horizontal pressure gradients in the free atmosphere, a katabatic circulation has developed in the lowest 3 km of the atmosphere after one martian day. It is clear that the radiative flux divergence in the atmosphere acts to influence nearly the entire martian atmosphere. This is considerably different from the Antarctic simulations and is a direct result of the thin martian atmosphere. Even relatively modest values of radiative flux divergence can lead to appreciable temperature change over time and hence the establishment of horizontal pressure gradients.

Figure 1b illustrates the vertical temperature profile in the lowest 3 km for the five cases considered. Pronounced inversion conditions prevail over a deep atmospheric layer. The exponential shapes of the temperature profiles are similar to those seen over the interior of Antarctica although the vertical scale of the martian profiles are much greater than found on Earth. Note that no significant difference is seen in the thermal structure for the five cases despite the fact that the terrain slopes and intensity of the katabatic wind regimes vary considerably. This again underscores the dominance of the radiation budget in forcing the thermal structure on Mars.

Influence of solar forcing on the martian drainage flows. To test the sensitivity of the martian slope flows to solar forcing, numerical experiments have been conducted in which the full cycle of solar forcing is replicated over sloping terrain. Results for a constant slope of 0.008 at 75° latitude will be described.

Five numerical simulations have been conducted covering the seasonal range of solar declination angles (24°, 12°, 0°, −12°, and −24°); the model equations are integrated for three complete martian days to allow the model to settle into a stable diurnal oscillation. The results presented here are taken from day 2; only minor variations were seen beyond the first diurnal cycle. It is assumed that the polar cap is composed of "dirty" ice with an albedo of 0.50. All simulations start from a rest state. Thus the influence of large-scale pressure gradients in the free atmosphere is neglected. This implies that all atmospheric motions arise due to the longwave radiative cooling or solar heating of the sloping terrain. No solar insolation is allowed for the first 12 hr of model integration time to allow the drainage flows to become established before model sunrise.

Figure 2 illustrates the diurnal course of the surface temperature, wind speed, and wind direction over the 0.008 slope martian terrain for solar declinations of 24°, 12°, 0°, −12°, and −24°, corresponding to curves A, B, C, D, and E respectively. Here the martian day is divided into 24 martian hours. Note that the Sun never sets during the midsummer period (Fig. 2a, curve A) and never rises for the winter case. The ground temperature (Fig. 2b) undergoes diurnal oscillations of 30 K in summer, with the magnitude of the oscillation decreasing with the approach of the autumn; the diurnal

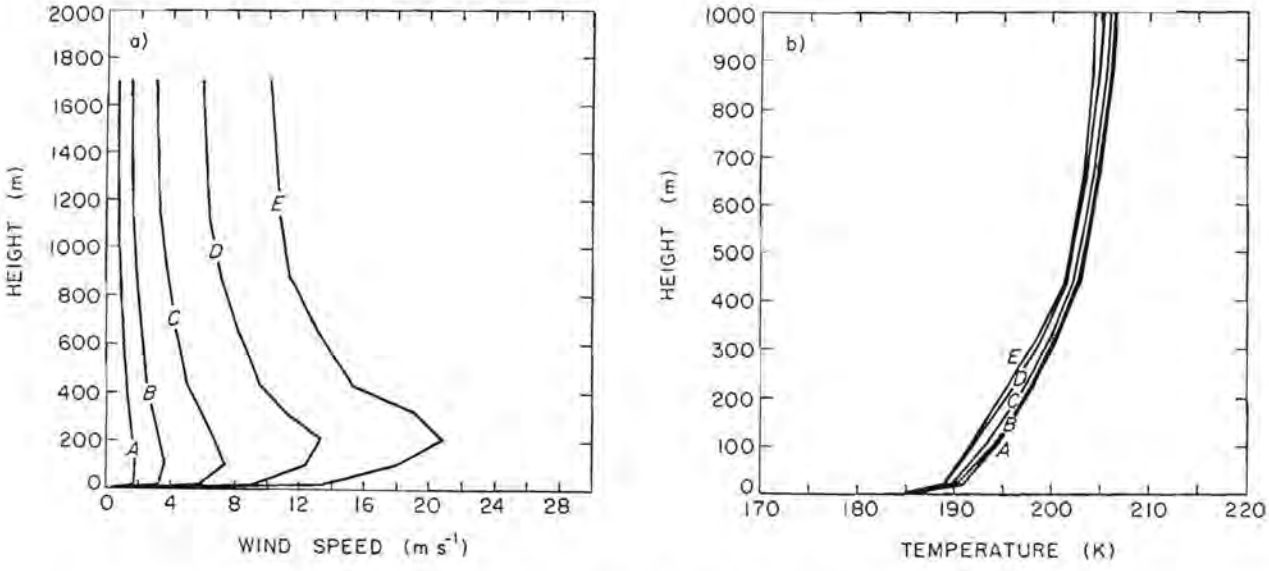

Fig. 1. Vertical profiles of (a) wind speed and (b) temperature in the lowest 3 km after 24-hr integration of constant slope runs.

ground temperature oscillation amounts to 15 K at the equinox. Maximum temperatures appear an hour or so after local noon. Wind speeds at the first sigma level corresponding to approximately 22 m above the surface (Fig. 2c) show marked diurnal trends during summer and equinox periods. Maximum wind speeds occur in the early morning hours coinciding with a minimum in the solar insolation in midsummer or just before sunrise in other simulations. Note that the simulated midsummer katabatic wind maximum of approximately 10.5 ms^{-1} (reached in the early morning hours) is 3 ms^{-1} less than seen for the other cases. This reflects the insolation from the midnight Sun, which retards development of the katabatic wind. Wind directions at the first sigma level throughout the diurnal course for the five numerical simulations are shown in Fig. 2d. The downslope direction is 180° for these simulations. The Coriolis force acts to deflect the katabatic wind some 30° to the right of the fall line of the terrain for the winter katabatic wind case. The wind directions show surprisingly little variation with time except for the midsummer declination angle of 24° (curve A). Note that upslope flow is modeled during the early afternoon hours of the summer case. The effect of solar insolation appears to retard but not overcome the katabatic forcing in all but the summertime case. This emphasizes the robust nature of the martian katabatic circulation.

Although the most pronounced diurnal changes occur near the surface, significant oscillations can be traced well into the atmosphere. In particular, the strong solar heating of the terrain results in a well-mixed boundary layer that extends upward of 2 km or so by early afternoon. Figure 3 illustrates the vertical structure of temperature and wind speed in the lowest 3 km for the five 0.008 slope experiments at 0200 LT and

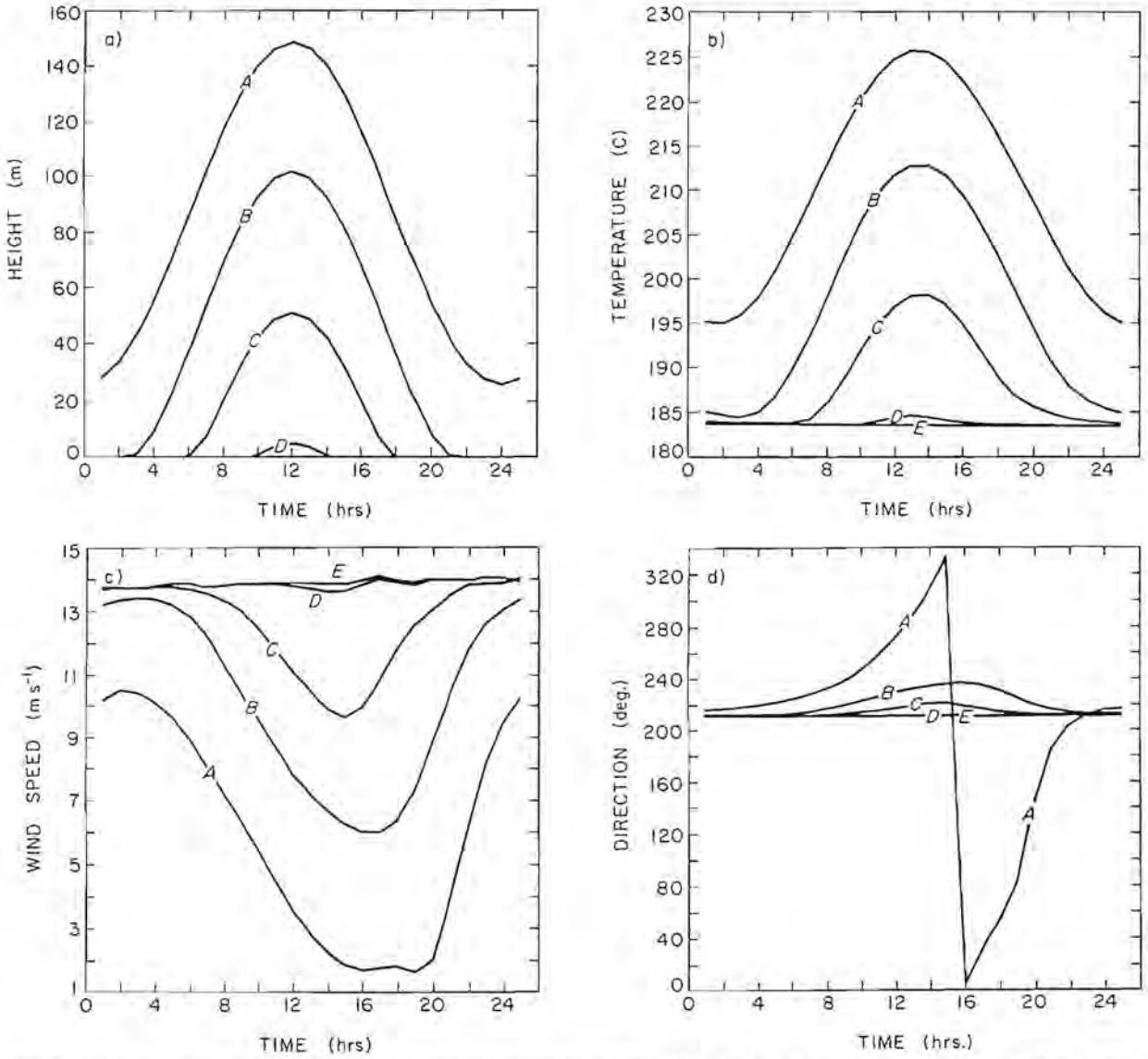

Fig. 2. Diurnal variation of (**a**) solar insolation reaching the ground, (**b**) ground temperature, (**c**) wind speed, and (**d**) wind direction at the lowest sigma level for the solar cycle simulations over the 0.008 slope.

1200 LT. The temperature profile for the early morning (Fig. 3a) shows an inversion structure for each simulation including the midsummer case (curve A) in which the Sun remains above the horizon for the entire martian day. Although relatively minor diurnal changes are seen above 1 km, seasonal temperature differences are evident. The midsummer thermal structure suggests a near-adiabatic profile above the inversion. The atmospheric stability above the katabatic layer increases as the intensity of solar radiation decreases such that by the equinox, inversion conditions prevail. The thermal structure of the atmosphere at noon (Fig. 3b) indicates adiabatic conditions prevail up to around 2 km during midsummer. The wind speeds (Figs. 3c,d) for the 0.008 slope show well-developed katabatic wind profiles during the early morning hours, although the intensity of the drainage flow is reduced considerably for the midsummer case. Wind speeds at local noon for the five solar declinations suggest that the katabatic wind regime in the lower atmosphere is considerably reduced by solar radiation during the nonwinter periods. The katabatic wind signature is still present in all but the midsummer case. Little diurnal variation is seen above 1 km.

Summary: Numerical simulations suggest katabatic winds are ubiquitous features of the nocturnal lower boundary layer at high latitudes on Mars. The drainage flows are analogous to those seen over the Antarctic continent, and have comparable scales of wind speeds and depths. Model experiments suggest that longwave radiative cooling is the dominant forcing mechanism for the martian katabatic winds and is responsible for establishing a horizontal pressure gradient in a deep layer over sloping terrain. The intensity of the induced circulation is dependent on the slope of the underlying terrain.

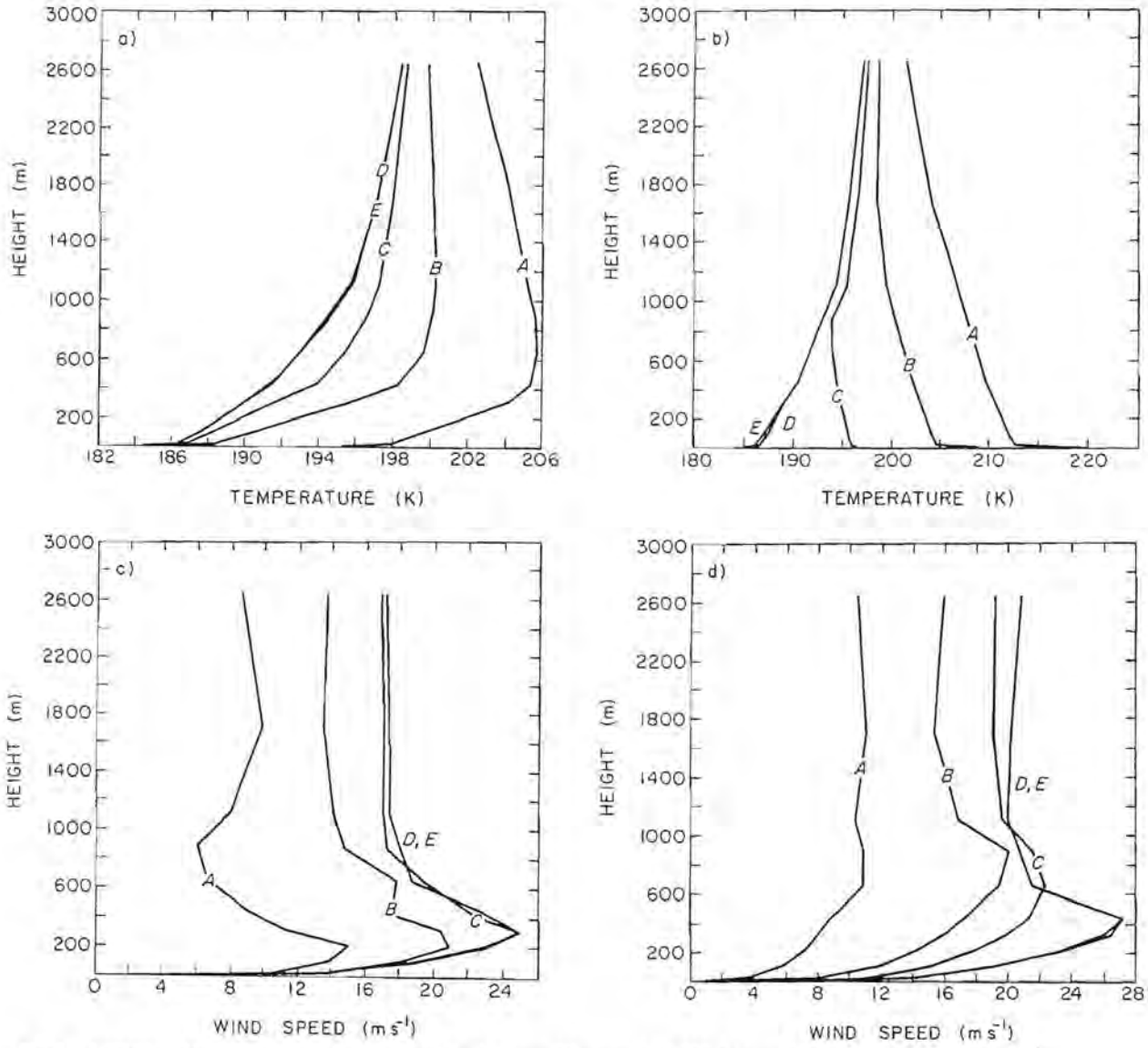

Fig. 3. Vertical profiles of temperature and wind speed in the lowest 3 km over the 0.008 slope at 0200 LT (left) and 1200 LT (right).

Model experiments incorporating the solar cycle show the katabatic wind to be completely suppressed only during the midsummer daytime simulation. The adjustment time for the development of the katabatic wind is quite short; during the early morning hours of midsummer the drainage flows are able to develop. This implies that once the Sun sets, the development of the katabatic wind is very rapid and near-steady conditions prevail in just a few hours.

References: [1] Hess S. L. et al. (1977) *JGR, 82,* 4559–4574. [2] Howard A. D. (1981) *NASA TM-82385,* 333–335. [3] Parish T. R. and Bromwich D. H. (1987) *Nature, 328,* 51–54. [4] Anthes R. A. and Warner T. T. (1978) *Mon. Wea. Rev., 106,* 1045–1078. [5] Parish T. R. and Waight K. T. (1987) *Mon. Wea. Rev., 115,* 2214–2226. [6] Brost R. A. and Wyngaard J. C. (1978) *J. Atmos. Sci., 35,* 1427–1440. [7] Busch N. E. et al. (1976) *J. Appl. Meteor., 15,* 909–919. [8] Businger J. A. et al. (1971) *J. Atmos. Sci., 28,* 181–189.

ANTARCTIC LAKES (ABOVE AND BENEATH THE ICE SHEET): ANALOGUES FOR MARS. J. W. Rice Jr., Astrogeology Branch, U.S. Geological Survey, Flagstaff AZ 86001, USA.

The perennial ice-covered lakes of the Antarctic are considered to be excellent analogues to lakes that once existed on Mars. Field investigations of ice-covered lakes, paleolakes, and polar beaches have been conducted in the Bunger Hills Oasis, Eastern Antarctica. These studies will also be extended to the Dry Valleys, Western Antarctica, and the Arctic.

Important distinctions have been made between ice-covered and non-ice-covered bodies of water in terms of the geomorphic signatures produced. Field investigations have revealed that the classical lacustrine landforms created by non-ice-covered lakes (spits, bars, berms, cusps, tombolos, and wave-cut platforms) are absent in an ice-covered lake regime. The features mentioned above are the result of the direct coupling of wind and the free water surface. The ice cover acts as a geomorphically protective agent. Therefore, the shores of ice-covered bodies of water are low-energy environments, i.e., poorly sorted, due to restricted or nonexistent wave action.

The most notable landforms produced by ice-covered lakes are ice-shoved ridges. These features form discrete segmented ramparts of boulders and sediments pushed up along the shores of lakes/seas. The shorelines are generally planated with the ramparts defining the inner edge of the shoreline. These ridges usually have a heterogeneous veneer of boulders, pebbles, sand, and gravel mantling an ice core. The ice core normally melts out and leaves behind its mantle of material in the form of irregular discontinuous ridges. The ice core can persist for years if it is sufficently insulated by its mantle of material.

The ice-shoved features observed in the Bunger Hills Oasis were up to 83 m long, 2 m high, and 4 m wide. Ice-shoved ridges up to 300 m long and 10 m high have been reported [1]. Other unique landforms associated with polar beaches are frost cracks and mounds, patterned ground, pingos, pitted beaches, coastal striated bedrock, and ventifacts. Investigations of ice-covered lakes in Antarctica has also disclosed information that may have important exobiological implications [2–4], namely the discovery of modern, cold-water, blue-green algal stromatolites that are adapted to extremely cold temperatures, fresh-to-saline water, and low light intensities, and the fact that an ice cover acts as both insulating blanket and protective seal for the liquid water located below. The ice cover's "sealing effect" allows the liquid water to retain biologically important gases that are dissolved in the water column.

Several paleolacustrine basins have been located and mapped on Mars [5,6]. The last vestiges of these martian lakes, which eventually froze throughout because the influx of meltwater ceased, are expected to be found at high latitudes. Provided that the ice cover was covered with the appropriate sediment thickness [7], these paleolake remnants would form a massive lens of buried ice. It is proposed that this lacustrine ice lens would be composed of interlayered fluvial/lacustrine sediment and ice. This layering would be created by the influx of sediment brought in by multiple flow episodes from channels located along the periphery of the basin [8–10]. Aeolian deposits would also contribute to the ice cover mantling. More investigative studies and field work will be conducted on these problems.

Sub-Ice-Sheet Lakes: Sub-ice lakes have been discovered [11] under the Antarctic ice sheet using radio echo sounding. These lakes occur in regions of low surface slope, low surface accumulations, and low ice velocity, and occupy bedrock hollows.

The development of Radio Echo Sounding (RES) in the late 1950s was driven by the necessity to measure ice thickness in a rapid, accurate, and continuous manner. RES provides information on electrical properties in ice, enables the study of ice-sheet surface form, thickness, internal structure, dynamics, thermodynamics, and basal conditions and processes [12].

Most of the lakes beneath the Antarctic ice sheet are located near Dome C in Eastern Antarctica [11]. Several very large lakes, up to 8000 km^2, have been discovered [12]. RES studies do not allow the depth of these lakes to be determined; however, the minimum thickness of a fresh-water layer can be estimated by the skin depth necessary for radio reflection [12]. Some of these lakes may have a minimum depth of 6.5 m.

The sub-ice lakes of Antarctica may have formed more than 5 m.y. ago [11]. This age is based upon deep-sea cores taken in the Ross Sea that indicate that the main Antarctic ice sheet has changed little in size since a retreat some 5 m.y.

ago [13]. The existence of these polar lakes may provide yet another oasis for life. Once basal melting of the ice sheet started, it would supply a slow but steady influx of microorganisms deposited in the past on the surface of the ice [11].

The presence of sub-ice lakes below the martian polar caps is possible. Calculations [14] suggest that basal melting is currently an active process in the polar regions. It has even been suggested [15] that the catastrophic drainage of basal lakes formed Chasma Boreal.

The discovery of the Antarctic sub-ice lakes raises intriguing possibilities concerning martian lakes and exobiology. The polar regions of Mars, like those on Earth, may preserve organic compounds [16]. Dark organic-rich carbonaceous chondrites would melt, sink, and be buried in the ice. The burial process would protect the meteorites from decomposition. It is conceivable that the sub-ice lakes may provide a refuge for any microorganisms, which either survived the downward passage through the ice or existed before the emplacement of the ice. I agree with Clifford [14] and propose that a RES be flown on a future mission to provide information on the martian ice bedrock interface: ice thickness, internal structure, basal conditions and processes, and thermodynamics. RES techniques used in the Antarctic are capable of measuring ice thicknesses greater than 4 km. This would be capable of penetrating martian polar ice thicknesses.

References: [1] Bretz J. H. (1935) *Am. Geog. Soc. Spec. Pub., 18,* 159–245. [2] Parker B. C. et al. (1981) *Bioscience, 31,* 656–661. [3] Wharton R. A. et al. (1987) *Nature, 325,* 343–345. [4] McKay C. P. and Davis W. L. (1991) *Icarus, 90,* 214–221. [5] Scott D. H. et al. (1991) *Origin Life Evol. Biosphere, 21,* 189–198. [6] Parker T. J. et al. (1989) *Icarus, 82,* 111–45. [7] Carr M. H. (1990) *Icarus, 87,* 210–227. [8] Rice J. W. and DeHon R. A. (1992) *Geologic Map of the Darvel Quadrangle, Maja Valles, Mars, scale 1:500,000,* in press. [9] Rice J. W. (1989) *Proc. LPSC 20th,* 898–899. [10] Scott D. H. and Dohm J. M. (1990) *Proc. LPS, Vol. 21,* 1115–1116. [11] Oswald G. K. and Robin G. D. (1973) *Nature, 245,* 251–254. [12] Drewry D. J. (1981) In *Remote Sensing in Meteorology, Oceanography, and Hydrology,* 270–284. [13] Hayes D. E. (1973) *Geotimes, 18,* 19. [14] Clifford S. M. (1987) *Proc. LPSC 14th,* in *JGR, 92,* B9135–B9152. [15] Clifford S. M. (1980) *Bull. Am. Astron. Soc., 12,* 678. [16] Pang K. et al. (1978) *2nd Colloquium on Planetary Water and Polar Processes,* 199–201.

MARS OBSERVER RADIO SCIENCE (MORS) OBSERVATIONS IN POLAR REGIONS

Richard A. Simpson, Center for Radar Astronomy, Stanford University, Stanford CA 94305-4055, USA.

Mars Observer Radio Science observations will focus on two major areas of study: (1) the gravity field of Mars and its interpretation in terms of internal structure and history and (2) the structure of the atmosphere, with emphasis on both temperature-pressure profiles of the background atmosphere and small-scale inhomogeneities resulting from turbulence (Fig. 1) [1]. Scattering of centimeter-wavelength radio signals from Mars' surface at highly oblique angles will also be studied during the primary mission; nongrazing scattering experiments may be possible during an extended mission. Aspects of each of these investigations will have implications for polar studies, especially since the radio path preferentially probes polar regions.

During the Mars Observer primary mission, measurements of the spacecraft distance and velocity with respect to Earth-based tracking stations will be used to develop models of the global gravity field. Doppler measurement accuracy is expected to be better than 0.1 mm/s for 10-s observation times; the resulting uncertainties in model coefficients will be comparable to or less than the values of the coefficients for all degrees less than about 50 (Fig. 2). The corresponding lateral resolution at the surface for fields of degree and order 50 should be about 220 km, leading to an order of magnitude improvement in knowledge of Mars' gravity field.

The improvement in knowledge of the gravity field will be especially evident in polar regions. The near-circular, near-polar orbit provides much better measurements at high latitudes than previous spacecraft orbits, which were ellipical and had periapses near Mars' equator. Study of long tracking arcs and evolution of the orbit through the two-year nominal Mars Observer mission may allow derivation of solar tidal forces exerted on the planet; the main tidal component likely to be sensed results in orbit perturbations with a period of about half of one of Mars' years. Seasonal variations in model coefficients resulting from redistribution of CO_2 between polar caps and the atmosphere are near the detection limit. Secular variations in J_2 may also be detected if Mars is not in hydrostatic equilibrium and the planet's shape is continuing to evolve.

The spatial and temporal coverage of atmospheric radio occultation measurements are determined by the geometry of the spacecraft orbit and the direction to Earth. The low-

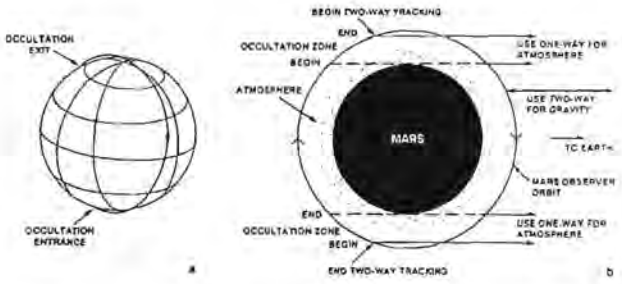

Fig. 1. Mars Observer geometry for Radio Science investigations. **(a)** Typical view from Earth when view angle is approximately 40° out of the orbit plane. **(b)** Sketch showing partition of orbit for gravity and atmospheric occultation observations.

altitude orbit during Mars Observer mapping remains Sun synchronous, but the view angle from an Earth receiving station can be as much as 60° out of the orbit plane. Although there is a period during 1995 when occultations at mid-latitudes can be observed, most of the Mars Observer experiments will take place at latitudes poleward of 60° (Fig. 3). Rotation of the planet between successive orbits will allow systematic measurements at regular intervals spaced by about 29° in longitude, alternating between northern and southern hemispheres.

Profiles of atmospheric temperature and pressure will extend from the surface to altitudes of 50–70 km. Atmospheric dust and haze have little effect on propagation of the radio wave; changes in opacity that lead to different profiles should be easily seen in the radio data provided that the perturbed region lies along the occultation path (Fig. 4). Polar phenomena that may be sensed include warmings that accompany global dust storms, reductions in CO_2 vapor pressure associated with condensation, and atmospheric waves. Of particular interest will be the structure of the atmosphere during periods when polar hoods form and the effect of the hood on radiative balance in the region covered.

Nominal vertical resolution for the radio occultation profiles is 100–200 m. If high-resolution analysis techniques—such as those that have been applied in ring occultations at Saturn and Uranus—can be adapted to the Mars Observer data, artifacts of the limb diffraction may be removed and resolutions as small as 10–20 m attained. The planetary boundary layer plays an important role in CO_2, H_2O, dust, and heat exchanges between the surface and atmosphere; occultation profiles at fine vertical resolutions will provide unique visibility into the thermal structure of this important region. Steep temperature inversions (20 K) observed in the lowest few kilometers above the polar cap in the spring season of each hemisphere and low temperatures associated with sublimation/condensation of CO_2 may be observed using the high-resolution techniques.

Obliquely scattered signals from the surface may complicate the high-resolution analysis of atmospheric occultation data; these echos must be identified, characterized, and removed before the compensation for effects associated with limb diffraction can be accomplished. In the process it may be possible to relate the properties of the scattered signal to surface texture and density. Scattering at near-grazing angles is not well understood, however; conventional scattering models developed for quasispecular processes do not account for the shadowing and diffraction expected at highly oblique angles.

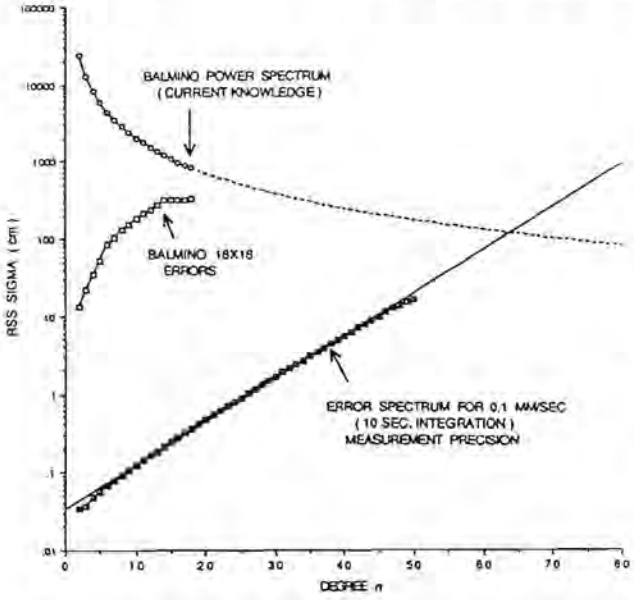

Fig. 2. Current gravity model ("Balmino power spectrum") extrapolated to higher degrees, current model uncertainties ("Balmino 18 × 18 errors"), and expected uncertainties from Mars Observer observations. Uncertainties are expected to remain below model coefficients for at least $n < 50$.

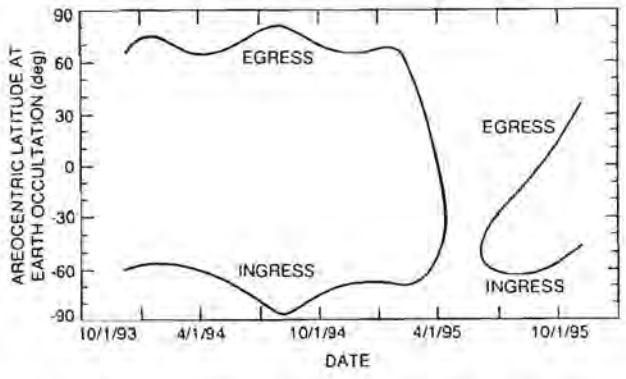

Fig. 3. Latitudinal coverage of atmospheric occultations for the nominal mapping orbit. Until early 1995, all occultation points will be poleward of 60° latitude.

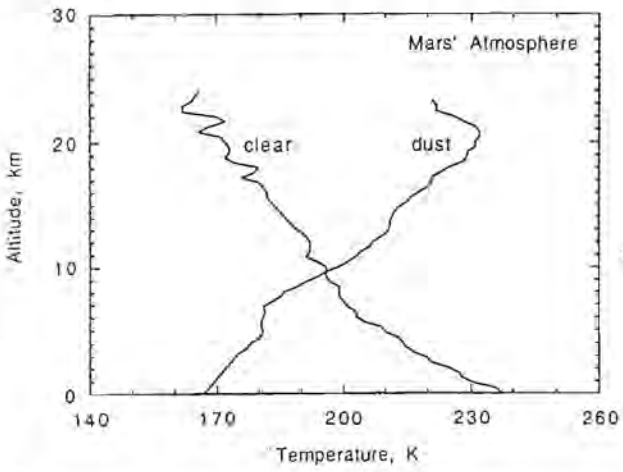

Fig. 4. Atmospheric temperature profiles from Viking radio observations [2]. The dramatic difference in temperature structure can be attributed to dust loading and increased optical opacity during the winter solstice global dust storm of 1977.

Obliquely scattered echos from the north polar cap near Chasma Boreale showed the surface to be usually smooth during experiments performed with Viking Orbiter 2; if the icy surface is typically smoother than Mars plains on scales of centimeters to meters, the modeling needed for occultation corrections may be simpler than anticipated.

Backscattering experiments on icy planetary surfaces have yielded unusually high radar cross sections and unpredicted polarizations. The Galilean satellites of Jupiter, for example, return more energy toward Earth-based radar systems than is expected from polished metal spheres of the same dimensions. They also return signals with predominantly the same polarizations as transmitted, counter to expectations based on simple reflection mechanisms for smooth surfaces. The same behavior has been seen in radar echos from the residual south polar cap on Mars. Oblique scattering experiments in which the Mars Observer antenna is aimed toward icy surface targets rather than in its nominal Earth-point direction may allow measurements of the scattered signal under conditions that will allow estimation of scattering path lengths within the ice, an important parameter in determining the composition and history of the ice itself.

References: [1] Tyler G. L. et al. (1992) *JGR, 97,* 7759–7779. [2] Lindal G. F. et al. (1979) *JGR, 84,* 8443–8456.

WIND TRANSPORT NEAR THE POLES OF MARS: TIMESCALES OF CHANGES IN DEPOSITION AND EROSION. Peter C. Thomas, Center for Radiophysics and Space Research, Cornell University, Ithaca NY 14853, USA.

Movement of sediment into and out of polar deposits is intimately linked to the polar volatile budget and to changes in wind systems over the course of astronomically induced climate cycles. Our present observations of the morphology of polar layered deposits, mantling sediments, dune fields, and variable surface features are the basis of inferences on the efficacy of polar sediment transport mechanisms. The timescales of formation of these features vary from days to perhaps 10^6 yr, and latitudinal banding of dune fields near the poles may have been formed on timescales of 10^7 yr.

Orientations of intracrater dunes, dune crests, and wind streaks have been measured for latitudes –45 to –90 to compare features of likely different timescales of formation with models of wind flow from the south polar region. The larger features, such as intracrater dune fields, suggest formation primarily by winds flowing out from the pole with both prograde and retrograde components. The very long timescales of formation expected of the dune fields are consistent with their formation by strongest winds at different parts of the cycle of season of perihelion. The bedforms superposed on the dune fields, however, suggest winds somewhat less varied than those apparently recorded by the dune fields, and more closely correlated with orientations of streaks from crater splotches and dune fields. This suggests that some bedforms of scales of about 100 m can be reoriented within one half of a cycle of season of perihelion (25,000 yr).

There is a complex variation with latitude of the indicated wind directions and of the efficacy of the resultant winds in orienting dune fields that suggests influence of frost cover on the ability of winds to move sediment in the spring and fall. Because of changes in the relative effectiveness of spring and fall winds expected with progression of the season of perihelion, the latitudinal variation in transport efficiency may mean that sediments at different latitudes dominantly respond to wind erosion and transport at different times during the perihelion cycle. The Viking data are too scattered in time to derive the controls on efficacy of fall and spring winds in detail, but monitoring by Mars Observer should allow generation of models of wind transport from and to the polar areas that may be extrapolated (with caution) to other parts of expected climate cycles. The likely long-term sedimentary balance of the polar deposits may then be more readily addressed.

MODELING INTERANNUAL VARIABILITY IN THE MARTIAN SEASONAL CO_2 CYCLE. S. E. Wood and D. A. Paige, Department of Earth and Space Sciences, University of California, Los Angeles CA 90024, USA.

One of the most intriguing aspects of the seasonal pressure variations measured at the Viking Lander sites is their nearly perfect interannual repeatability [1,2]. This presents something of a problem, because it implies that the behavior of the seasonal polar caps should be highly repeatable from year to year as well. There are a number of observations and theories suggesting that the presence of dust and water ice clouds in the martian atmosphere should have significant direct and indirect effects on the rates of CO_2 condensation and sublimation in the north and south polar regions. These effects include (1) reduced rates of CO_2 frost condensation during polar night seasons due to the radiative effects of dust and water ice clouds [3–6] and associated CO_2 clouds [7,8] or elevated atmospheric temperatures [9,10] and (2) reduced or elevated rates of frost sublimation due to the radiative effects of atmospheric dust [6,11,12], or to changes in frost emissivities and albedos due to contamination by water ice and dust [8,13–15]. Because all these effects rely on the transportation of dust, water, and heat into the polar regions by the martian atmosphere, they are not expected to be exactly repeatable from year to year, especially given that two global dust storms were observed during the first Viking year, and none were observed the second and third [1,2,16]. Since all these effects could potentially contribute to the asymmetrical behavior of CO_2 frost at the north and south residual polar caps observed during the first Viking year

[12,17–19], assessing their impact on the present seasonal CO_2 cycle is of importance not only for understanding martian interannual climate variations, but long-term climate variations as well.

In this paper, we first examine the Viking Lander pressure observations themselves to determine the range and character of the interannual variations present. Then we use a diurnal and seasonal thermal model described by Wood and Paige [20] to quantitatively examine the effects of interannual variations in the polar heat balance on seasonal pressure variations.

Viking Lander Interannual Pressure Differences: Viking Landers 1 and 2 (VL1 and VL2) obtained surface pressure measurements during parts of four and two Mars years respectively [2]. We have examined the VL1 and VL2 daily averaged pressure data to determine the seasons and magnitudes of possible long-period interannual pressure variations [21]. At VL1, interannual pressure differences were typically less than 5 Pa from L_s 0 to L_s 180, but variability increased significantly between L_s 180 and L_s 360 [21]. During the 1977B global dust storm, average VL1 pressures were over 20 Pa higher than they were during the third year. The interannual pressure differences observed at VL2 show similar general trends to those observed at VL1, but the magnitudes are almost doubled [21]. Observed interannual pressure differences at VL2 were less than 5 Pa from L_s 120 to 180, but exceeded 20 Pa during the subsiding phases of the 1977A global dust storm, and exceeded 50 Pa during 1977B [21].

Overall, the results suggest that the interannual variability present in the Viking Lander pressure data may be due as much to interannual differences in atmospheric thermal and dynamic structure as to differences in atmospheric mass. An interannual variation in atmospheric mass would be expected to result in a pressure difference of the same sign at both landing sites. The large differences in average pressures that were observed during the 1977B global dust storm must also be partially due to atmospheric dynamic phenomena [22–24]. Despite potential ambiguities in their interpretation, the observed interannual pressure differences at the Viking Lander sites still place strong constraints on the potential magnitudes on interannual variations in the heat balance of the martian seasonal polar caps. In the following sections we take the observed VL1 interannual pressure differences as upper limits for interannual variations in the mass of the martian atmosphere.

Sensitivity to Year-Long Heat Balance Variations: Our experiences fitting the Viking pressure data [20] indicate that the martian seasonal pressure variations are extremely sensitive to year-long variations in the heat balance of the north and south seasonal polar caps. To demonstrate, we ran our diurnal and seasonal thermal model [20] for a number of years using a set of "standard best-fit" model input parameters that simultaneously fit the VL1 third-year seasonal pressure data and the retreat rates of the north and south seasonal polar caps. Then we slightly altered the values of the best-fit albedos or emissivities of the seasonal frost deposits in either hemisphere through a complete cycle of polar cap growth and retreat. The results are presented in Table 1, which summarizes the standard best-fit model parameters, the alterations that were introduced, and the resulting maximum interannual pressure variations.

The results suggest that a uniform persistent interannual variation in the albedo or emissivity of the north or south seasonal polar cap of greater than 2% absolute would be quite apparent in the Viking Lander pressure data. Larger year-long interannual variations in the parameters could potentially be compatible with the available observations, but only if they occurred over limited periods of time and/or limited portions of the seasonal polar caps. Interannual pressure variations of these magnitudes would not be expected to produce large interannual variations in polar cap retreat rates.

TABLE 1. Year-long variations.

Parameter Changed	"Standard Best-fit" Value*	Perturbation Value	Max. Pressure Deviation	L_s of Peak
North Albedo	0.70	0.67	+10	50
North Emissivity	0.69	0.72	−11	12
South Albedo	0.54	0.51	+11	215
South Emissivity	0.71	0.68	+16	160

*Based on "standard best-fit" model using a total mass of CO_2 in the cap-atmosphere system of 210 kg/m^2, thermal inertia of soil in the northern hemisphere equal to 670 (MKS), and 167 (MKS) in the south.

Sensitivity to North Polar Warming: Both the Mariner 9 IRIS and Viking IRTM instruments observed significantly elevated atmospheric temperatures over the north seasonal polar cap during the 1971A and 1977B global dust storms [9,10]. For the case of the 1977B storm, IRTM 15-μm channel brightness temperatures exceeded 230 K at the edge of the polar night. Martin and Kieffer [10] have considered the downward flux of infrared radiation at the surface of the north seasonal polar cap due to these elevated atmospheric temperatures, and concluded that CO_2 condensation rates were substantially reduced for the cap as a whole during the peak of the storm. Near the edge of the cap, elevated atmospheric temperatures may have caused net CO_2 sublimation, amounting to perhaps as much as 13 Pa of CO_2 gas, globally averaged [10], which would be roughly consistent with the pressure increase observed at VL2.

Our thermal model [20] can be used to investigate some of the implications of the hypothesis that north polar cap CO_2 frost condensation was briefly halted during the 1977B storm. Figure 1 shows model-calculated surface pressures and north polar cap boundaries after a number of years of calculations

using the standard best-fit parameters, except during winter of the last year, when the emissivity of the entire north polar cap was decreased from 0.69 to 0.25 starting at L_s 280, and then increased back to 0.69 after 20 days. This effectively halts net frost condensation on the north seasonal cap as a whole during the period when elevated IRTM 15-μm channel brightness temperatures were observed. Lowering the emissivity to zero would have resulted in net sublimation since the outer portions of the cap are outside the polar night.

As can be seen in Fig. 1, a brief cessation of frost condensation during the peak of the second global dust storm would have resulted in significantly elevated surface pressures at both landing sites that would not have disappeared until L_s 80 when the north seasonal polar cap had completely sublimated. If the north polar cap actually lost mass during the peak of the dust storm, the long-term effects on pressure would be greater still. This means that the true net effects of the elevated atmospheric temperatures on the heat balance of the north polar cap must have been smaller than estimated here, or these effects "healed" later in the winter due to increased frost condensation rates. Similar constraints must also apply to alternate mechanisms for reducing CO_2 frost condensation rates during the polar night that could exhibit interannual variability, such as the formation of atmospheric CO_2 clouds [7,8].

Sensitivity to North Polar Dust Contamination: Soon after the Viking discovery of the asymmetric behavior of seasonal frost at the north and south residual caps, it was pointed out that dust raised in the southern hemisphere during global dust storms could be transported northward and deposited onto the condensing north seasonal frost deposits, and lower the albedo of the polar cap during the following spring [25]. Pollack et al. [26] have estimated that as much as 0.02 g cm^{-2} yr^{-1} of dust was deposited north of +60° latitude during the first Viking year. Toon et al. [13] have calculated that only half this amount could lower pure frost albedos from 0.7 to 0.55. Warren et al. [14] have shown that depending on assumptions, the incorporation of dust into martian seasonal frost deposits could have even larger effects.

The potential effects of dust contamination on the behavior of the north seasonal polar cap can also be investigated using our thermal model [20]. The results presented in Table 1 show that a small year-long decrease in the albedo of either seasonal cap would have caused significant persistent interannual pressure variations. However, the results of these simulations may not be directly applicable to the situation where a layer of dark, dust-contaminated frost is deposited onto the condensing north seasonal polar cap during a global dust storm. Since such a dust layer would soon be covered by uncontaminated CO_2 frost, its effect on the polar cap's heat balance should not be apparent until most of the overlying uncontaminated CO_2 frost had sublimated. Figure 2 shows the results of a simulation where we ran the thermal model for a number of years using the standard best-fit model input

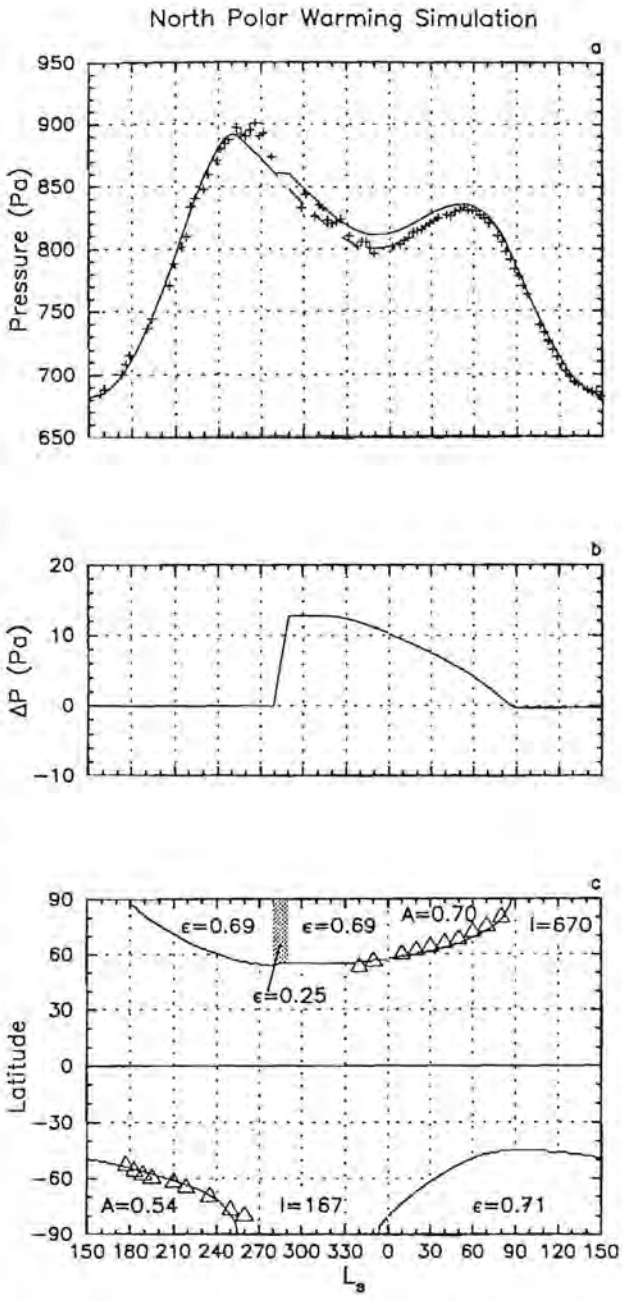

Fig. 1. (a) Model-calculated surface pressures (solid line) compared to VL1 year 3 binned data (pluses). The "standard best-fit" parameters [A = frost albedo, ε = frost emissivity, I = soil thermal inertia (MKS)] were used until the last year when the north seasonal polar cap CO_2 frost emissivity was lowered to 0.25 from L_s 280 to 290.5 to simulate north polar warming during the 1977B global dust storm. Dashed line indicates unperturbed "standard best-fit" pressure curve. (b) Interannual variation in atmospheric pressure calculated by subtracting the best-fit pressure curve from the perturbed model-calculated pressures. The pressure difference increased at a constant slope until the emissivity was reset to 0.69. (c) Latitudinal extent of model-calculated seasonal polar caps and Viking Orbiter observations (triangles) of the retreating cap edges in 1977 [27,28] shown for comparison.

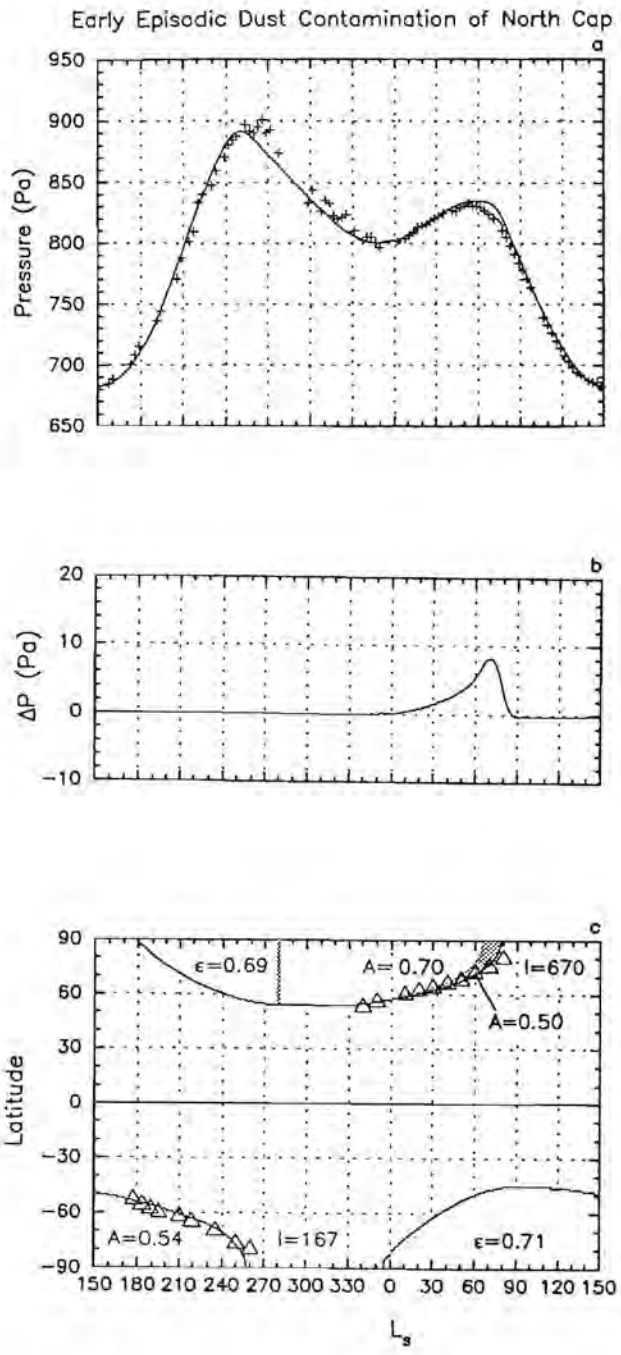

Fig. 2. Same format as Fig. 1. The "standard best-fit" parameters were used, but a "dust layer" was deposited onto the condensing north seasonal polar cap at L_s 280 with the initial phase of 1977B, then gradually exposed by sublimation of overlying CO_2 frost in the spring. This contaminated frost (indicated by shaded region after it is uncovered) was assumed to reduce the frost albedo from 0.70 to 0.50, resulting in higher sublimation rates. Although the observed pressure difference (**b**) is smaller than that resulting from the year-long 3% north polar cap albedo decrease indicated in Table 1, the effect on the retreat rate is slightly greater, causing the north seasonal cap (**c**) to disappear before L_s 80.

parameters, but during the winter of the final year, a dust layer was deposited onto the condensing north polar cap. The timing of the dust layer's deposition was assumed to coincide with the polar warming event associated with the initial phases of the 1977B dust storm at L_s 280. As the cap retreated during spring, the dust layer became exposed at the surface of the frost, first at the edge of the cap, and finally over the entire cap during the final stages of the retreat. Wherever the dust layer was exposed, seasonal frost albedos were assumed to decrease from their best-fit values of 0.7 to 0.5, and then were assumed to remain at 0.5 until the frost completely sublimated. The computed interannual pressure differences for this simulation increased charply as the cap approached the final phase of retreat, but never exceeded 10 Pa. When compared to the first case listed in Table 1, the results presented in Fig. 2 are somewhat surprising, given the large changes in frost albedos that are assumed. We also performed other simulations for dust layers deposited later in the season, and found that the magnitudes of the computed pressure changes are larger because less frost forms over them and the dust is uncovered earlier.

Although these simulations are highly idealized, they demonstrate that the effects of episodic dust contamination events on the seasonal pressure curves may not be nearly as significant as expected. The signatures of these episodes on interannual pressure variations are peaked during the final retreat phases of the contaminated polar cap. Although incomplete, the VL1 data show no real indication of sustained elevated pressures during mid to late northern spring in any of the Viking years, and no evidence of the distinctive peak in interannual pressure differences during late spring. However, based on the amount of interannual variability present in the data, we estimate that these observations could potentially be compatible with the deposition of a dust layer at L_s 280 that had a spring season darkening effect of as much as 10% absolute. For a dust layer deposited at L_s 310, the darkening could be no more than 4% absolute. Since a difference between albedos of seasonal frost deposits at the north and south poles of this order could result in the observed asymmetry of the behavior of CO_2 frost at the north and south poles, the repeatability of the Viking seasonal pressure curves may not necessarily be incompatible with contamination of the accumulating north seasonal polar cap during global dust storms. Based on polar radiation balance measurements, Paige and Ingersoll [12] have estimated that the entire asymmetry can be explained by an approximately 20% absolute difference between the late spring albedos of the CO_2 frost deposits at the north and south residual polar caps. While it is not known whether this north-south difference is due entirely to differential dust contamination during global dust storms, the results of this study do not necessarily preclude this possibility.

References: [1] Leovy C. B. et al. (1985) *Recent Advances in Planetary Meteorology* (G. E. Hunt, ed.), 19–44, Cambridge, New York. [2] Tillman J. E. (1988) *JGR, 93,*

9433–9451. [3] Leovy C. B. (1966) *Science, 154,* 1178–1179. [4] Briggs G. A. (1974) *Icarus, 23,* 167–191. [5] James P. B. and North G. R. (1982) *JGR, 87,* 10271–10283. [6] Lindner B. L. (1990) *JGR, 95,* 1367–1379. [7] Paige D. A. (1985) Ph.D. dissertation, California Institute of Technology, Pasadena. [8] Pollack J. B. et al. (1990) *JGR, 95,* 1447–1473. [9] Hanel R. A. et al. (1972) *Science, 175,* 305–308. [10] Martin T. Z. and Kieffer H. H. (1979) *JGR, 84,* 2843–2852. [11] Davies D. W. (1979) *JGR, 84,* 8335–8340. [12] Paige D. A. and Ingersoll A. P. (1985) *Science, 228,* 1160–1168. [13] Toon O. B. et al. (1980) *Icarus, 44,* 552–607. [14] Warren S. G. et al. (1990) *JGR, 95,* 14717–14741. [15] James P. B. et al. (1990) *JGR, 95,* 1337–1341. [16] Colburn D. S. et al. (1988) *NASA TM-100057.* [17] Kieffer H. H. et al. (1976) *Science, 194,* 1341–1344. [18] Farmer C. B. et al. (1976) *Science, 194,* 1339–1341. [19] Kieffer H. H. (1979) *JGR, 84,* 8263–8288. [20] Wood S. E. and Paige D. A. (1992) *Icarus, 99,* 1–14. [21] Paige D. A. and Wood S. E. (1992) *Icarus, 99,* 15–27. [22] Haberle R. M. et al. (1982) *Icarus, 50,* 322–367. [23] Zurek R. W. (1982) *Icarus, 50,* 288–310. [24] Zurek R. W. and Haberle R. M. (1988) *J. Atmos. Sci., 45,* 2469–2485. [25] Kieffer H. H. and Palluconi F. D. (1979) *2nd International Colloq. on Mars,* NASA CP-2072, 45–46. [26] Pollack J. B. et al. (1979) *JGR, 84,* 2929–2945. [27] James P. B. et al. (1979) *JGR, 84,* 2889–2922. [28] James P. B. (1979) *JGR, 84,* 8332–8334.